Article

Cell Host & Microbe

Recruitment of Adult Precursor Cells Underlies Limited Repair of the Infected Larval Midgut in *Drosophila*

Graphical Abstract

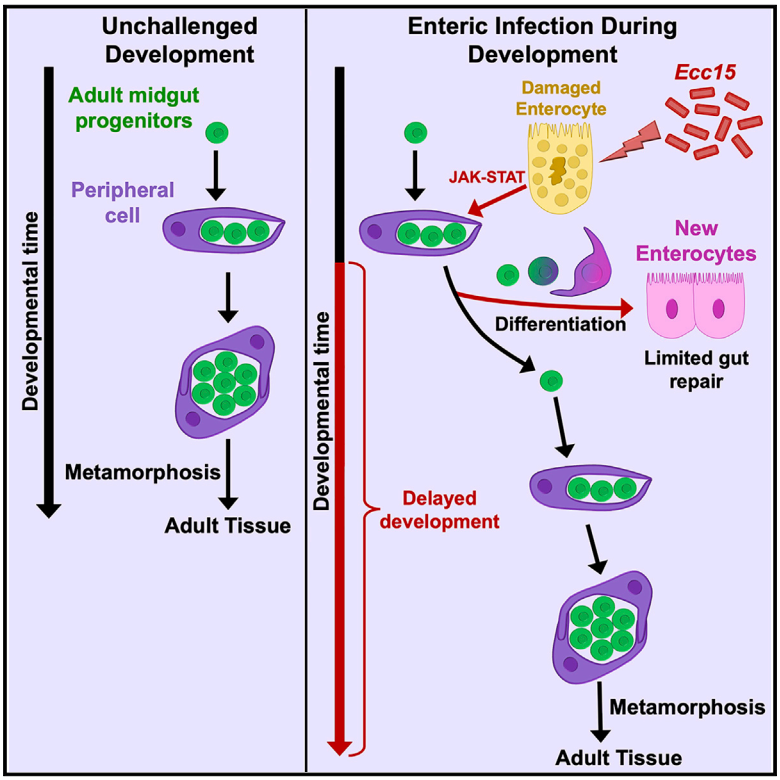

Highlights

- Oral infection is more dramatic in larvae than adults and induces developmental delay
- Larval gut repair is limited and achieved by differentiation of adult gut precursors
- Developmental delay allows for reconstitution of the pool of adult midgut precursors
- The JAK-STAT pathway is induced by infection and controls precursor differentiation

Authors

Philip Houtz, Alessandro Bonfini, Xiaoli Bing, Nicolas Buchon

Correspondence

nicolas.buchon@cornell.edu

In Brief

Houtz et al. find larval *Drosophila* circumvent the lack of stem cells through controlled differentiation of adult midgut progenitor cells to mediate partial renewal following enteric bacterial damage. A concurrent delay in larval development allows the pool of progenitors to be reconstituted by cells that were not diverted for repair.

Houtz et al., 2019, Cell Host & Microbe *26*, 412–425
September 11, 2019
https://doi.org/10.1016/j.chom.2019.08.006

CellPress

CellPress

Cell Host & Microbe
Article

Recruitment of Adult Precursor Cells Underlies Limited Repair of the Infected Larval Midgut in *Drosophila*

Philip Houtz,[1] Alessandro Bonfini,[1] Xiaoli Bing,[1] and Nicolas Buchon[1,2,*]
[1]Cornell Institute of Host-Microbe Interactions and Disease, Department of Entomology, Cornell University, 129 Garden Ave., Ithaca, NY 14853, USA
[2]Lead Contact
*Correspondence: nicolas.buchon@cornell.edu
https://doi.org/10.1016/j.chom.2019.08.006

SUMMARY

Surviving infection requires immune and repair mechanisms. Developing organisms face the additional challenge of integrating these mechanisms with tightly controlled developmental processes. The larval *Drosophila* midgut lacks dedicated intestinal stem cells. We show that, upon infection, larvae perform limited repair using adult midgut precursors (AMPs). AMPs differentiate in response to damage to generate new enterocytes, transiently depleting their pool. Developmental delay allows for AMP reconstitution, ensuring the completion of metamorphosis. Notch signaling is required for the differentiation of AMPs into the encasing, niche-like peripheral cells (PCs), but not to differentiate PCs into enterocytes. Dpp (TGF-β) signaling is sufficient, but not necessary, to induce PC differentiation into enterocytes. Infection-induced JAK-STAT pathway is both required and sufficient for differentiation of AMPs and PCs into new enterocytes. Altogether, this work highlights the constraints imposed by development on an organism's response to infection and demonstrates the transient use of adult precursors for tissue repair.

INTRODUCTION

Organisms require robust developmental processes to ensure their viable transition into adults. The tightly regulated progression of development can interfere with the regenerative capacity of maturing organisms. This suggests that the ability of developing organisms to deal with damage, injury, or stress could be particularly constrained. Organisms have developed strategies to cope with such challenges. In *Drosophila melanogaster* larvae for instance, undifferentiated and fate-committed imaginal cells, which are precursor cells for adult appendages, have ingrained repair processes that allow for their reconstitution when damaged (Hariharan and Serras, 2017; Smith-Bolton, 2016; Smith-Bolton et al., 2009). Damaged imaginal tissue alters developmental timing via cellular signaling that ultimately modulates the circulating levels of hormones such as PTTH, in order to coordinate the repair with developmental progression (Colombani et al., 2012; Halme et al., 2010; Jaszczak et al., 2016). However, it remains unclear whether damage to the larval tissue itself triggers a similar regenerative process as well as if and how it may impact development. This is especially important for the intestinal epithelium, which faces the unique challenge of balancing digestive and absorptive functions with its role as a barrier to ingested pathogenic microbes and harmful chemicals (Buchon et al., 2013). In this study, we analyze the larval gut epithelial response after oral pathogenic infection, its impact on adult midgut precursor cells, and the consequences that this has on the gut and organismal development.

Preservation of tissue homeostasis and epithelial integrity in the gastrointestinal tract requires continual tissue turnover, enacted in the digestive tract via the proliferation and differentiation of dedicated intestinal stem cells (ISCs) to counter the constant loss of old, damaged, or dying epithelial cells. Tissue renewal is also crucial for the gut to mend itself in response to infectious, chemical, or physical injuries (Karin and Clevers, 2016; Liu et al., 2017). The *Drosophila* larval midgut epithelium contains absorptive enterocytes (ECs) and secretory enteroendocrine cells (EEs). However, in contrast with its adult counterpart, it does not undergo continuous epithelial renewal (Jiang and Edgar, 2009; Micchelli et al., 2011). Accordingly, during larval development, the midgut does not grow in size by increasing the number of ECs, but rather by increasing the size and ploidy of a set number of larval ECs (Duronio, 1999). Additionally, the larval midgut contains undifferentiated progenitor cells, the adult midgut precursors (AMPs) that ultimately generate all of the epithelial cells in the adult midgut (Mathur et al., 2010). AMPs undergo several rounds of division over the course of larval development to form distinct structures akin to imaginal discs known as imaginal midgut islets. These islets consist of a central cluster of proliferating AMPs enclosed within the membrane(s) of one or more surrounding peripheral cells (PCs) and are dispersed throughout the larval midgut epithelium (Mathur et al., 2010). PCs act as a barrier to enclose AMPs and actively control their behavior, thus acting as a temporary niche.

The digestive tract of *Drosophila* larvae is exposed to a continuous flow of ingested material that can contain potentially pathogenic microbes, since its natural diet is composed of yeasts and other microbes growing in rotting fruits (Lemaitre and Hoffmann, 2007). Most bacteria are non-infectious upon ingestion

and rapidly eliminated from the gut, but a few pathogens have been identified that can persist in the larval midgut, elicit a systemic immune response, and perturb epithelial homeostasis. These include *Erwinia carotovora ssp carotovora 15* (*Ecc15*), a gram-negative plant pathogen, that was discovered to also be pathogenic to *Drosophila melanogaster* larvae, a characteristic conferred by the *Erwinia virulence factor* (*evf*) (Acosta Muniz et al., 2007; Basset et al., 2003). *Drosophila* employs multiple strategies to combat oral infection, including the secretion of antimicrobial peptides under the control of the Imd pathway, the production of reactive oxygen species by NADPH oxidases such as Nox and Duox as well as behavioral adaptations (Bae et al., 2010; Buchon et al., 2009b). For instance, in response to infection, hosts can speed up food bolus passage through the gut (Du et al., 2016) or decrease the ingestion of contaminated food (Soldano et al., 2016; Stensmyr et al., 2012). *Drosophila* larvae can detect the presence of *Ecc15* via olfaction and respond by decreasing food uptake (Keita et al., 2017). *Ecc15* ingestion impedes larval growth by inhibiting commensal bacteria-enhanced protein digestion (Erkosar et al., 2015). *Ecc15* is also pathogenic to adult *Drosophila*, in which it induces a massive loss of ECs when ingested and subsequently triggers an increase in stem cell-mediated tissue turnover (Bonfini et al., 2016; Buchon et al., 2009a, 2009b). Tissue repair is essential to survive the enteric infection and requires coordination of multiple signaling pathways including the JAK-STAT, EGFR, Wnt, and TGF-β/Dpp pathways (Bonfini et al., 2016; Houtz et al., 2017). This posits the question: how does the larval gut reliably endure pathogenic injury without the support of ISC-mediated renewal?

In this study, we found that *Ecc15* damages the *Drosophila* larval midgut and, unlike in adults, is partially lethal to larvae. Larvae that survive infection display a developmental delay, possibly due to a decrease in digestion. Larvae fed *Ecc15* experienced epithelial damage, causing the gut to shrink in length. However, tissue repair via AMP and PC differentiation into new ECs, allowed some larvae to survive the infection. Surprisingly, no increase in AMP proliferation accompanies differentiation, thus stunting the accumulation of AMPs needed for metamorphosis. A developmental delay induced by infection allowed the pool of AMPs to be reconstituted, an essential component to resume development. We determined that the Notch pathway, which is required for the differentiation of AMPs into PCs, is not sufficient to drive differentiation into ECs. Furthermore, we demonstrate that AMP differentiation depends on JAK-STAT signaling, initiated by the release of cytokines from stressed ECs. Altogether, our results demonstrate how infection transiently diverts adult precursors from their developmental task to execute the repair needed to allow host survival of infectious damage.

RESULTS

Ecc15 Infection Induces Partial Lethality and a Developmental Delay in *Drosophila* Larvae

To explore differences in the outcome of pathogenic infections on adult and developing hosts, we orally infected *Drosophila* adult females and 2nd instar (L2) larvae with *Ecc15*. As previously reported (Buchon et al., 2009b), adult flies survived this infection without a detectable impact on their lifespan (Figure 1A), a phenomenon attributable to the ability of the adult midgut to regenerate lost cells upon infection, via ISC activity (Buchon et al., 2009a, 2009b, 2010). This homeostatic ability can be overcome by a strain of *Ecc15* that overexpresses the virulence factor *evf* (*pOM evf*). Ingestion of this strain was lethal in 20% of the flies, suggesting a competition between bacterial virulence and tissue repair (Figure 1A). By contrast, in larvae, even wildtype *Ecc15* induced mortality at doses as low as OD_{600} = 16 (70% lethality). *evf* overexpression increased the lethality to ~95% (Figure 1B). To determine if larvae are broadly more vulnerable than adults to enteric damage, we recorded the survival of larvae and adults after ingesting mild doses of the insect pathogens *Pseudomonas entomophila*, *Pseudomonas aeruginosa*, and *Providencia rettgeri* as well as after feeding on 1% SDS (Figure S1A). Adult survival did not fall below 80% within a week of any of the treatments, but larval survival was significantly lower in all cases and dropped to ~30% on *P. entomophila* and ~50% on *P. aeruginosa*. These results demonstrate that larvae are broadly more susceptible than adults to oral pathogenic infections.

To characterize larval vulnerability to enteric pathogens, we assessed the developmental stage at which lethality occurs. We found that most infected larvae (up to 60%) died prior to pupation (between L2 and yellow pupa (YP); L, Figure 1C). Surviving larvae took 2–4 days longer (depending on the dose) than unchallenged (UC) to reach adult eclosion following treatment (Figure 1B). To determine if this developmental delay affects a particular stage, we measured the number of days spent in each stage and found that only the transition time from L2 larvae to pupation is lengthened, while the duration of the YP and black pupal (BP) stages remained unchanged between infected and UC groups (Figure 1D). In addition, the YP weight of larvae either infected with *Ecc15* or unchallenged was not different, suggesting they reach their target mass before engaging in pupation (Figure S1B). Finally, the adult lifespan of flies that survived through metamorphosis following larval infection was not altered from that of UC flies (Figure 1E). Altogether, these results imply that the larval stage is more susceptible to *Ecc15* infection, but that survivors are able to resume normal development and adult life after a delay at the larval stage.

It was previously shown that oral *Ecc15* infection triggers food uptake blockage in larvae (Acosta Muniz et al., 2007; Keita et al., 2017). The resulting nutrient deprivation may explain the susceptibility of larvae to infection as well as the developmental delay in survivors. To test this hypothesis, we assayed food intake in larvae exposed to *Ecc15* and in agreement with previous work, observed a feeding cessation dependent on the virulence factor *evf* (Figure 1F). *Ecc15*-infected larvae resumed feeding within 4 h post-infection but at a decreased rate (Figure S1C). In addition, the amount of food detected in the guts of infected larvae was significantly lower when compared to UC larvae (Figure S1D). Thus, larvae ingesting *Ecc15* either die or experience a developmental delay prior to pupation, coincident with a reduction in feeding.

Damage to the Larval Midgut Is Repaired by Differentiation of Adult Midgut Progenitors

In adult *Drosophila*, *Ecc15* ingestion induces midgut epithelial cell loss, subsequently triggering ISC proliferation and differentiation

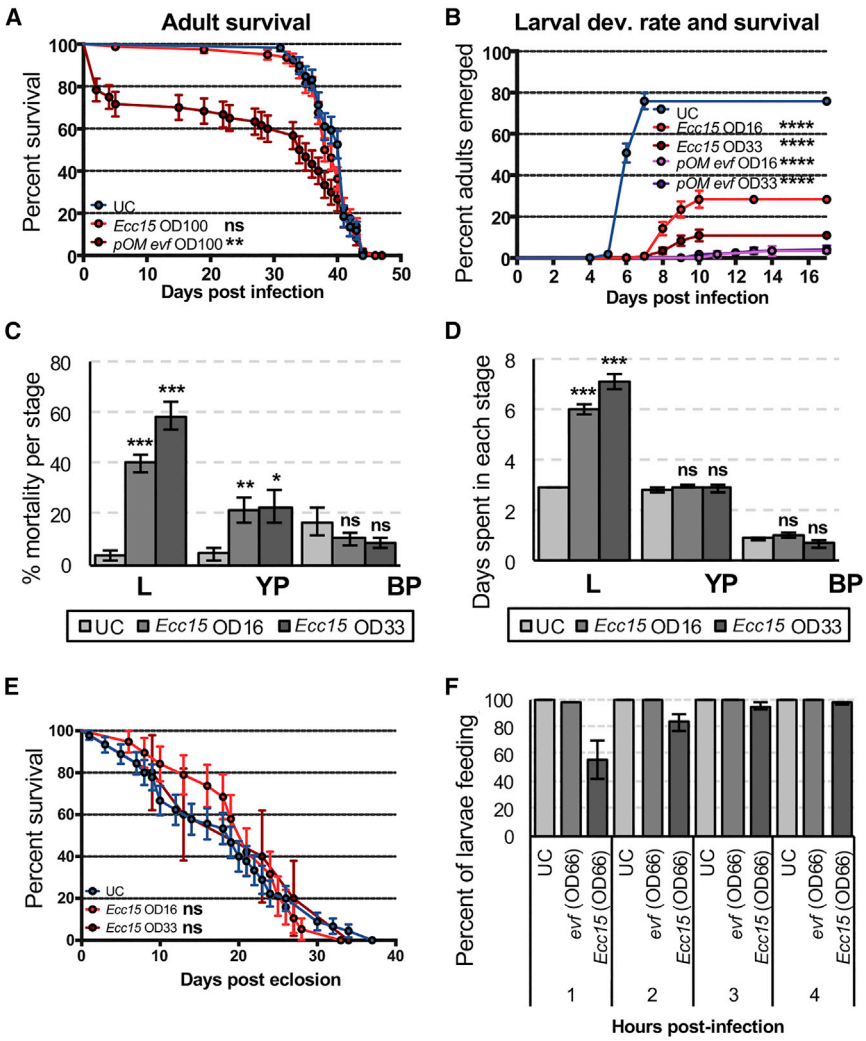

Figure 1. Oral *Ecc15* Infection of Larval *Drosophila* Induces Mortality and Developmental Delay

(A) *pOM-evf Ecc15*, but not wild-type *Ecc15*, decreases adult *Drosophila* survival upon oral infection.

(B) *Drosophila* larvae are susceptible to both wildtype and *pOM-evf Ecc15* and display delayed development to adulthood.

(C) Percentage of deaths occurring during the larval (L), yellow pupal (YP), and black pupal (BP) stages following infection shows that most lethality occurs in larvae and a fraction (~20%) during YP to BP transition.

(D) The average transition time from L2 larvae to YP, YP to BP, and BP to adult for larvae infected with two different doses of *Ecc15* shows that the developmental delay occurs in larval stages.

(E) Survival curves of adults that survived *Ecc15* infection as larvae show that larval infection does not affect the lifespan of surviving adults.

(F) Percentage of larvae ingesting blue fly food medium following oral infection shows that feeding resumes after a few hours. Statistical significance: mean values of at least 3 repeats are represented ± SEM. *p < 0.0332, **p < 0.0021, ***p < 0.0002, ****p < 0.0001 (compared to UC, Log-rank test for survival curves). *p < 0.05, **p < 0.01, ***p < 0.001 (compared to UC, Student's t test for transition period and mortality measurements).

See also Figure S1.

to produce new cells required for gut regeneration, which is critical to surviving infection (Liu et al., 2017). The larval midgut grows only by increasing the size and ploidy of ECs, while AMPs proliferate and accumulate in midgut imaginal islets during larval development and are only released at pupation to form the basis of the pupal and adult midgut epithelia (Mathur et al., 2010; Micchelli et al., 2011). Larvae, which lack dedicated tissue-resident stem cells, may then more easily succumb to enteric infection due to an inability to repair tissue using stem cells. To test this hypothesis, we investigated the effects of *Ecc15* infection on the midguts of *Drosophila* larvae. In UC conditions, the larval midgut is approximately 12 mm at the L2 and early 3rd instar (eL3) stages. Just before pupation, in the wandering L3 (wL3) stage, the gut shrinks (Figure 2A) by a process involving activation of autophagy to resorb larval tissue (Denton et al., 2009). As in adults, upon infection, the midgut shrunk by ~50%, similar to wL3 (Figure 2A), suggesting that *Ecc15* ingestion damages the larval midgut epithelium. This decrease in size could also explain the lower amount of food measured in infected larvae (Figure S1D). However, the larval midgut does not recover its size as in adults and instead remains shortened throughout larval maturation (Figure 2A). This lack of regeneration may indicate that the larval midgut is not able to repair infectious damage at all, or that repair is limited to maintaining the gut at a wL3 length.

To investigate these two possibilities, we monitored the larval midgut in detail for evidence of tissue renewal. We hypothesized that the AMPs, being a pool of undifferentiated progenitor cells, may temporarily act as tissue-resident stem cells to promote repair upon oral infection by *Ecc15*. To test this, we surveyed the lineage of AMPs and PCs (esg^+ cells) using the $esg^{F/O}$ system, which labels all esg^+ cells and their entire progeny in GFP (Jiang et al., 2009). Upon infection, AMP islets gave rise to GFP-positive, polyploid cells, which were not detected under UC conditions and expressed the EC-specific marker *Myo-lacZ*, suggesting that new ECs are generated from AMPs in response to infection (Figure 2B). The new ECs have smaller nuclei than pre-infection larval ECs, suggesting that they do not reach the same ploidy level (Figure 2B). In the adult midgut and other systems, stem cell-mediated tissue repair often pairs differentiation with increased stem cell proliferation in order to sustain regeneration (Bonfini et al., 2016; Buchon et al., 2009b; Jiang et al., 2009). To determine if tissue repair in the larval midgut is also accompanied by increased AMP proliferation, we measured the number of mitotic cells ($PH3^+$ cells) per larval midgut. Surprisingly, we found that the number of mitotically active AMPs (all $PH3^+$ cells were also esg^+) following infection was actually lower in infected L3 larvae compared to UC L3 larvae (Figure 2C). Altogether, our

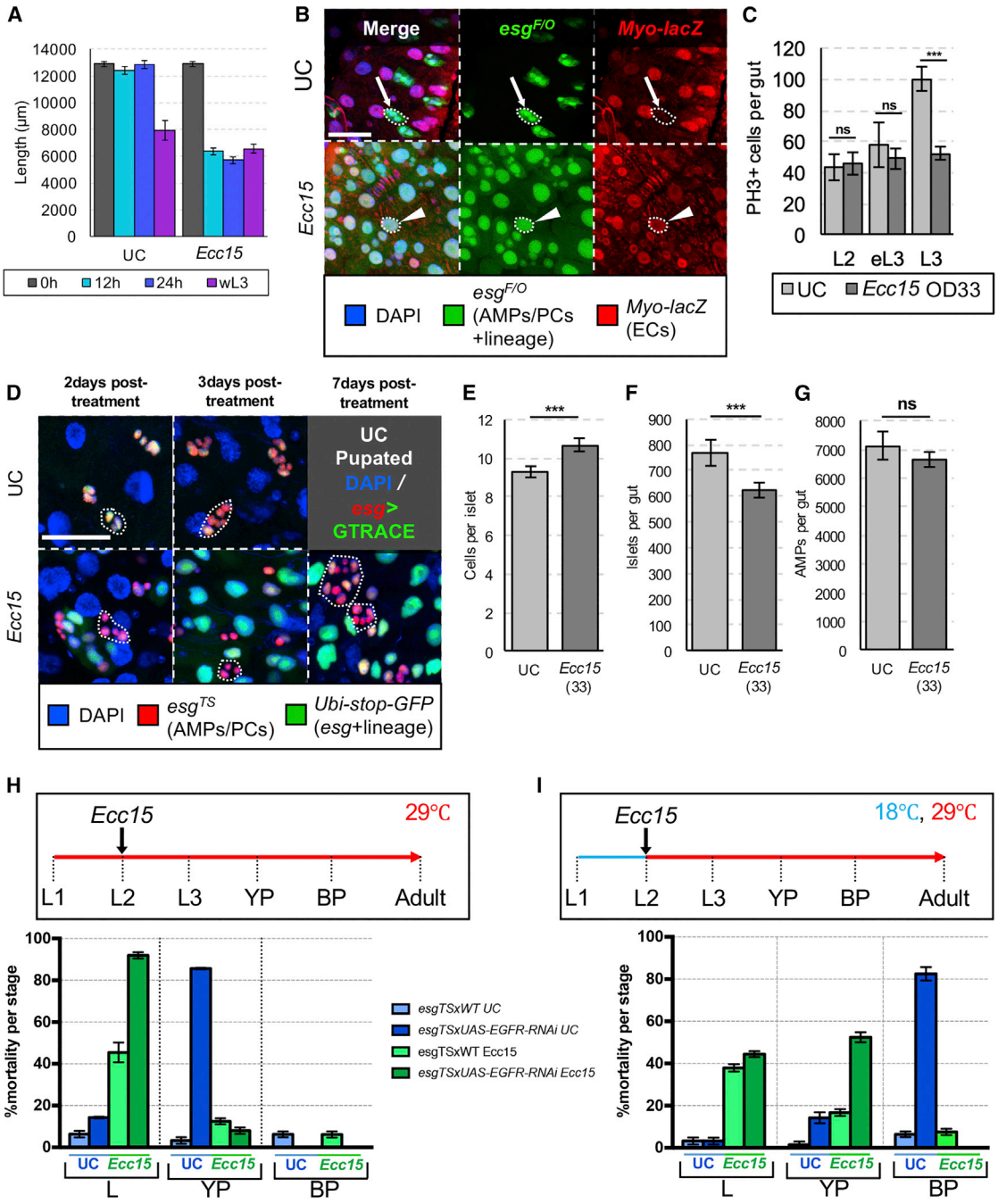

Figure 2. Infection of the Larval Midgut Triggers a Regenerative Response via AMP Differentiation

(A) Total midgut length measured 12, 24, and 96 h post-treatment in L3 larvae (UC flies pupate before 96 h). UC wL3 guts were dissected 72 h post-treatment, and infected wL3s were dissected at 96, 120, and 144 h and the lengths averaged.

(B) Lineage tracing of *esg*$^{+}$ AMP islets with *esg*$^{F/O}$ (green) reveals that AMPs undergo differentiation into ECs, marked by *Myo-lacz* (red), following *Ecc15* infection. Regions enclosed by dotted lines show UC islets (arrow) are *Myo-lacZ* negative, while newly differentiated ECs (*esg*$^{F/O+}$) are *Myo-lacZ* positive (arrowhead).

(C) Total number of mitotically active AMPs (PH3^{+}) does not increase for early stage larvae following infection (L2 and earlyL3), and decreases for L3 stage larvae that have been orally infected.

(D) G-TRACE lineage tracing shows that islet size is decreased compared to UC controls 2–3 days post-infection and returns to normal or greater size by 7 days post-infection. AMP islets are marked in red and green (examples enclosed by a dotted line), and their progeny marked in green.

(E–G) The number of cells in each islet (E), the total number of islets per midgut (F), and the total AMPs per gut (G) was recorded for wL3 larvae 3 days post-treatment for UC and 4–6 days post-treatment for the developmentally delayed infected group.

(legend continued on next page)

results demonstrate that differentiation of AMP islet cells in the absence of increased proliferation allows for a limited tissue repair response.

Since AMPs differentiate into new larval ECs following infection without a compensatory increase in proliferation, we hypothesized that the pool of AMPs might be depleted upon infection. Lineage tracing of islet cells with the *G-TRACE* system (Evans et al., 2009) allowed us to monitor simultaneously both the newly generated ECs (GFP^+ cells with polyploid nuclei) and the pool of undifferentiated AMPs (small RFP and GFP double-positive cells). After the first 3 days post-infection, the number of AMPs within islets was lower compared to those of UC larvae, and accordingly, the quantity of new ECs had increased within this time (Figures 2D, S2A, and S2B). By 7 days post-infection, however, the number of AMPs per islet appears to increase. Curiously, quantification of the number of AMPs per islet in wL3 larvae revealed that infected larvae had more AMPs per islet than UC larvae just prior to pupation (Figure 2E). Furthermore, the total number of islets in the guts of previously infected wL3 larvae decreased due to infection, indicating that roughly 150 islets on average were completely lost during regeneration (Figure 2F). As a result, the average number of total AMPs per midgut was ultimately unchanged at the time of pupation between UC and infected larvae (Figure 2G). Quantifying the dynamics of total midgut AMPs in UC and *Ecc15* infected larvae at the time of treatment, and across the L2, L3, and wL3 stages post-treatment, revealed that the total number of AMPs continuously increased during development in UC conditions. In contrast, the number of AMPs failed to increase in infected larvae until the wL3 stage (Figure S2C). Altogether, our data indicate that *Ecc15* infection triggers a transient induction of differentiation in AMPs to regenerate the larval midgut. This process competes with ongoing AMP proliferation and accumulation, but proliferation continues over the course of the infection-induced developmental delay allowing survivors to reach the same final number of AMPs as UC larvae by the wL3 stage.

To assess this model functionally, we manipulated the number of AMPs by modulating the EGFR-Ras-MAPK pathway, which is required for developmentally regulated islet proliferation (Jiang et al., 2011). We first induced the AMP proliferation by overexpressing in islet cells a constitutively active form of Ras (esg^{TS}>*UAS-Ras*^{V12}), an activator of the EGFR pathway. AMPs in these guts over-proliferated and formed tumor-like cell clusters, but did not become new ECs (i.e., polyploid cells) (Figure S2D), reinforcing the notion that tissue repair is mediated mostly by differentiation rather than proliferation. Blocking EGFR signaling in esg^+ cells (esg^{TS}>*UAS-EGFR-IR*) resulted in the loss of esg^+ and $PH3^+$ cells (Figures S2E and S2F), confirming a key role of this pathway in regulating AMP proliferation. These esg^{TS}>*EGFR-IR* larvae reached pupation at a normal rate despite the lower number of AMPs but subsequently died at the YP stage (Figures 2H and S2G). This demonstrated that the total number of AMPs per midgut does not act as a checkpoint to initiate pupation, but is nevertheless a critical factor for pupal midgut formation. Inhibiting AMP proliferation drastically reduced the number of *Ecc15*-infected larvae that survived to pupation (Figure 2H), suggesting that larval midgut repair, despite being limited, is crucial to endure infectious damage and is dependent on AMPs. Finally, we monitored the survival of larvae that were reared to the L3 stage normally but then had AMP proliferation blocked upon treatment and throughout the AMP recovery phase (switch to 29°C to activate EGFR-IR concomitant with infection, Figures 2I, S2H, and S2I). While UC larvae survived this treatment until the BP stage and developed at a normal rate, larvae infected with *Ecc15* died at the YP stage, suggesting that proliferation after the time of infection, and thus AMP recovery during developmental delay, is also critical for survival. Altogether these data imply that the AMP accumulation required to form the adult midgut epithelium is slowed by differentiation following enteric infection, and the developmental delay allows this pool to be replenished over time. This constrained tissue repair is nonetheless required to survive the infection and successfully undergo metamorphosis, as is the proliferation of AMPs during the developmental delay. However, while the delay allows for AMP recovery, the number of AMPs itself does not regulate time to pupation.

Infection Triggers Differentiation of PCs in a Notch-Independent Manner

As the midgut imaginal islets are composed of two cell types, the undifferentiated AMPs and the surrounding differentiated PCs, we next asked which of these cell types contribute to tissue repair upon infection. The differentiation of AMPs into PCs is dependent on Notch signaling and the Notch ligand, Delta, is a marker of AMPs while the Notch activation reporter *Su(H)-lacZ* marks PCs (Figures 3A and 3C) (Mathur et al., 2010). We observed that, during *Ecc15* infection, the typical enveloping shape of PCs appeared to be disrupted, and newly formed ECs were *Su(H)-lacZ*$^+$, suggesting that new ECs may be the result of further PC differentiation (Figure 3A). To test this hypothesis, we performed a pulse-chase lineage tracing of PCs using the $Su(H)^{F/O}$ system (*Su(H)-Gal4;UAS-GFP,tub-Gal80*^{TS} >*UAS-FLP, act>CD2>Gal4*), in which we labeled PCs with a heritable GFP prior to infection and only for a limited window of time. After infection, GFP-positive ECs were detected, demonstrating that infection triggers differentiation of PCs into ECs (Figure 3B).

As the Notch pathway is a key regulator of ISC differentiation in the adult *Drosophila* midgut (Ohlstein and Spradling, 2007), we hypothesized that levels of Notch pathway activity may control differentiation of AMPs and PCs into ECs. Accordingly, immunostaining against Delta combined with esg^{TS}>*UAS-mCherry* and *Su(H)-GFP*, as well as a $Delta^{TS}$>*GFP* line, demonstrated that the Notch pathway is upregulated in islets 12 h post-infection (Figures 3C and S3). Specifically, we observed that Delta levels increased in islets and that the Notch pathway (*Su(H)-GFP*) was induced in AMPs in addition to PCs (Figure 3C). Accordingly,

(H and I) Percentage of deaths occurring during the larval (L), yellow pupal (YP), and black pupal (BP) stages following infection (green) or UC treatment (blue) of Cs control and esg^{TS}-driven *EGFR-RNAi* larvae, in which RNAi expression was induced starting either from an early stage (H) or at the time of treatment (I). Nuclei are stained with DAPI (blue) throughout the figure. Images are representative of cells present in five or more guts per sample group in at least three replicates. Scale bars are 50 μm. Statistical significance: mean values of at least 3 repeats are represented ± SEM. *$p < 0.05$, **$p < 0.01$, ***$p < 0.001$ (Student's t test).
See also Figure S2.

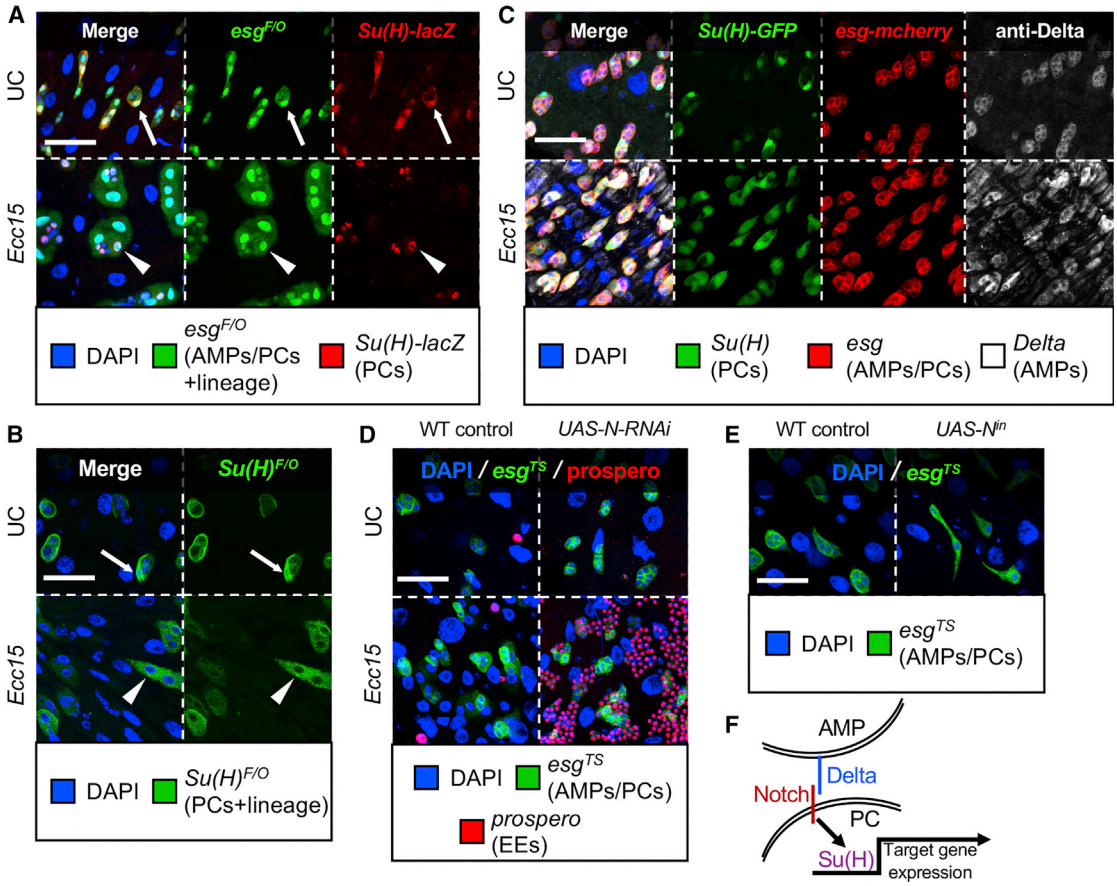

Figure 3. Notch Signaling Induces Adult Midgut Progenitors to Undergo Partial Differentiation into Peripheral Cells

(A) The Notch pathway is normally active in islet PCs (arrow), marked with *Su(H)-lacZ* (red), and is switched on in differentiating AMPs during regeneration (arrowhead). $esg^{F/0}$ labels AMPs, PCs, and their progeny (green).

(B) Transient induction of the $Su(H)^{F/O}$ system (green) in PCs (arrow) demonstrates that they contribute to midgut repair by differentiation into new ECs (arrowhead).

(C) Delta (white) localizes within AMP islets in both UC and *Ecc15*-infected guts and is increased by infection. Islets are marked with esg^{TS}>*UAS-RFP* (red), PCs are marked with *Su(H)-GFP* (green).

(D) RNAi knockdown of *Notch* causes AMP islets (esg^+, green) to lose their PCs in UC conditions and results in the formation of $Prospero^+$ (red) tumors upon *Ecc15* infection.

(E) Overexpression of the Notch intracellular domain (N^{in}) in AMPs (esg^+, green) causes differentiation into elongated, PC-like cells.

(F) A cartoon of the Notch signaling pathway. Nuclei are marked with DAPI (blue). Images are representative of cells in five or more guts per sample group in at least three replicates. Scale bars are 50 μm.

See also Figure S3.

blocking the Notch pathway in AMPs throughout early larval stages (esg^{TS}>*UAS-Notch-IR*) resulted in islets lacking PCs in UC conditions, and infection caused these Notch deficient islets to form *prospero*+ tumors instead of ECs (Figure 3D). This confirms that the Notch pathway is required for proper differentiation of AMPs into PCs and is a prerequisite for generating new ECs in response to *Ecc15* infection. Finally, activation of the Notch pathway in the AMPs of L2 larvae, via overexpression of the intracellular domain of Notch (esg^{TS}>*UAS-Notch-intra*), caused the differentiation of all AMPs into elongated, PC-like cells, but was not sufficient to induce further differentiation into polyploid ECs (Figure 3E). Altogether, our results suggest that, while Notch pathway activity is required for AMPs to differentiate into PCs and is triggered in response to *Ecc15* infection, it is not enough to promote differentiation of PCs into ECs (Figure 3F).

The Imd, Notch, DPP, and JAK-STAT Pathways Are Transcriptionally Upregulated in the Larval Midgut upon *Ecc15* Infection

Our results indicated that additional regulators are required to regulate islet differentiation upon *Ecc15* infection. To identify candidate genes for the promotion of islet differentiation, we compared adult and larval midgut transcriptomes in UC and *Ecc15*-infected conditions 6 h post-treatment. We first determined the overall transcriptomic differences between adult and larval guts in response to infection. 267 genes were upregulated in both adult and larval midguts following infection. Gene Ontology (GO) enrichment analysis revealed that these included genes involved in immune (Imd and JAK-STAT pathways) and stress (*p38c* and *p53*) responses as well as tissue regeneration (*Mmp1* and *NijA*) (Figures 4B, 4C, and S4A). 527 genes were

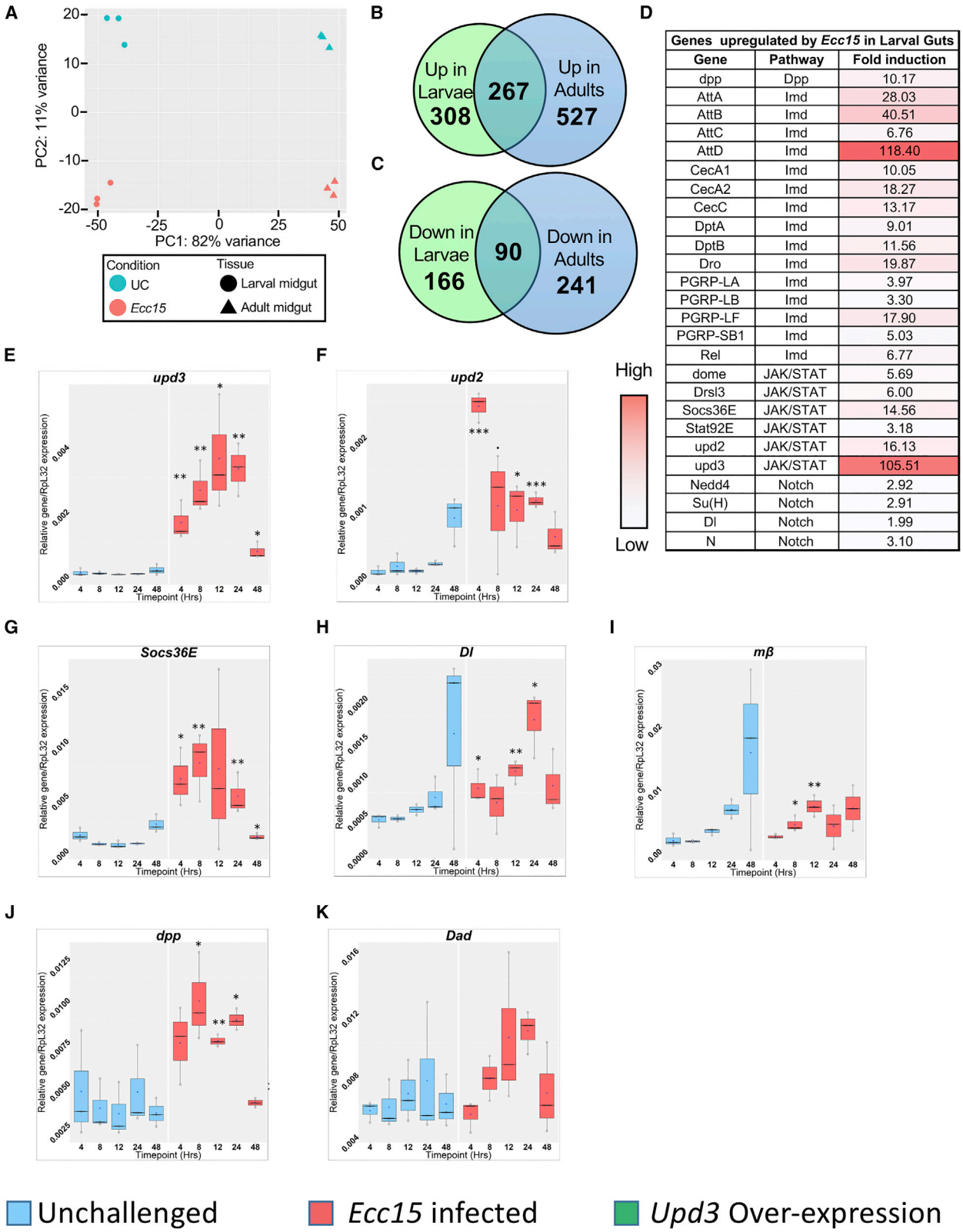

Genes upregulated by *Ecc15* in Larval Guts		
Gene	**Pathway**	**Fold induction**
dpp	Dpp	10.17
AttA	Imd	28.03
AttB	Imd	40.51
AttC	Imd	6.76
AttD	Imd	118.40
CecA1	Imd	10.05
CecA2	Imd	18.27
CecC	Imd	13.17
DptA	Imd	9.01
DptB	Imd	11.56
Dro	Imd	19.87
PGRP-LA	Imd	3.97
PGRP-LB	Imd	3.30
PGRP-LF	Imd	17.90
PGRP-SB1	Imd	5.03
Rel	Imd	6.77
dome	JAK/STAT	5.69
Drsl3	JAK/STAT	6.00
Socs36E	JAK/STAT	14.56
Stat92E	JAK/STAT	3.18
upd2	JAK/STAT	16.13
upd3	JAK/STAT	105.51
Nedd4	Notch	2.92
Su(H)	Notch	2.91
Dl	Notch	1.99
N	Notch	3.10

Figure 4. Activation of the Dpp, Imd, JAK-STAT, and Notch Pathways Defines a Core Response to Gut Infection in Both Adults and Larvae

(A) Principal component analysis (PCA) shows samples subjected to same treatment cluster together, indicating good repeatability. Most variance (PC1, 82%) is due to infection, while adult versus larval midgut contributes to 11% of the variance (PC2).

(legend continued on next page)

upregulated only in the adult midgut and included genes involved in cell cycle and DNA replication (*mus209 [PCNA]* and *hd*), reinforcing that ISC proliferation is increased upon infection in adult but not larval midguts. Finally, 308 genes were found to be uniquely upregulated in the larval midgut by infection and displayed an enrichment for functions in cell growth and differentiation (*Thor* and *Akt1*), in agreement with the induction of differentiation-mediated tissue repair. Upon infection, both larval and adult guts experienced a downregulation of genes involved in metabolism and digestion, suggesting a decrease in digestive capabilities (Figures S4A and S4D). Notably, the transcriptional downregulation of genes related to protein, lipid, and carbohydrate digestion in larvae upon infection (Figure S4D) could be causal for the infection-associated developmental delay.

We next focused on the most upregulated pathways of the larval gut upon infection, as potential controllers of the differentiation of AMPs and PCs into ECs (Figure 4D). As expected, one of the most upregulated pathways was the Imd pathway, a major branch of *Drosophila* immunity (Buchon et al., 2014). Additionally, in agreement with our previous results (Figures 3C and S3), we detected strong Notch pathway induction. Finally, we noted strong upregulation of two pathways that have been linked to stem cell differentiation in the adult midgut: the Dpp pathway (through upregulation of *dpp* itself) and the JAK-STAT pathway (identified via upregulation of the ligands *upd2* and *upd3* as well as the target gene *Socs36E*) (Beebe et al., 2010; Buchon et al., 2009a; Li et al., 2013a, 2013b; Zhai et al., 2017). We used qPCR to analyze the expression dynamics of key genes in the JAK-STAT, Notch, and Dpp pathways in larval midguts post-*Ecc15* infection (Figures 4E–4K). In UC conditions, the expression of JAK-STAT and Notch pathway genes increased over 48 h of development, while Dpp pathway gene expression stayed stable. Infection induced the expression of all three JAK-STAT pathway genes. *Dl* reached peak expression at 24 h and then decreased at 48 h, and *mβ* expression peaked at 12 h post-infection. *dpp* itself was induced above UC levels by 8 h post-infection before dropping back to UC levels by 48h, and levels of *Dad* expression did not significantly differ between the UC and infected groups across time points, albeit showing an increasing trend. Our results, therefore, suggest that Dpp and/or JAK-STAT may influence infection-induced AMP differentiation.

The Dpp Pathway Is Sufficient, but Not Necessary to Induce AMP Differentiation into ECs

The transcriptional upregulation of *dpp* by an infection in the larval *Drosophila* midgut was somewhat surprising, as previous research has suggested that Dpp is secreted by the PCs to maintain Dpp pathway activation in AMPs where it acts to prevent their differentiation (Mathur et al., 2010). However, Dpp pathway activation upon infection was confirmed via a *dpp-lacZ* reporter and antibody staining against phosphorylated Mad, the main Dpp pathway transcription factor (Figures 5A and 5B). We therefore, hypothesized that the Dpp pathway may counteract AMP differentiation in order to prevent complete AMP loss during repair. To test this, we first ectopically activated the Dpp pathway in islets by Dpp overexpression (esg^{TS}>*UAS-dpp*) and by overexpression of a constitutively active form of the Dpp receptor, Thickveins (esg^{TS}>$UAS\text{-}tkv^{CA}$). Both constructs caused AMPs to undergo differentiation into ECs (Figures 5C and 5D), suggesting that the Dpp pathway in AMPs, as in adult ISCs, promotes EC fate (Zhai et al., 2017). We then tested whether the Dpp pathway could be required for tissue renewal upon infection. However, blocking the pathway in AMPs by RNAi knockdown of *tkv* (esg^{FO}>*UAS-tkv-IR*), Mad ($esg^{F/O}$>*UAS-Mad-IR*), or punt ($esg^{F/O}$>*UAS-put-IR*) was insufficient to inhibit differentiation upon infection (Figures 5E and S5A). We found that MARCM clones carrying a tkv^{4} loss of function mutation likewise were not blocked from differentiation following infection (Figure S5B). These results suggest that while the Dpp pathway has the ability to promote AMP differentiation, it is not required to trigger differentiation upon infection.

The JAK-STAT Pathway Is Required and Sufficient to Trigger Infection-Induced Differentiation of AMPs into New ECs

To confirm the induction of the JAK-STAT pathway (Figure 6F) in the larval midgut upon infection, we monitored the expression of a *10xSTAT-GFP* reporter transgene (Figure 6A). Interestingly, no signal was detected in UC larval midguts at 4, 8, 12, or 24 h post-treatment. At the late L3 larval stage, however, the JAK-STAT pathway became active in islet cells (Figure S6A). Upon infection with *Ecc15*, *10xSTAT-GFP* signal was detected in both visceral muscles and in the differentiating AMPs of larvae as early as 4 h post-treatment, suggesting that JAK-STAT signaling is intensified and induced in additional midgut tissues following infectious damage. Furthermore, a β-galactosidase reporter for *upd3* (*upd3-lacZ*), a key ligand responsible for inducing the JAK-STAT pathway in response to infection (Houtz et al., 2017), distinctly showed transcriptional induction in the ECs surrounding differentiating AMP islets (Figure 6B). It was previously shown that two different enhancer regions of *upd3* (called *upd3* enhancers C and R) mediate the *upd3* transcriptional response to *Ecc15* infection of the adult gut (Houtz et al., 2017). We tested whether these same enhancers were activated by an infection in larvae (Figures S6B and S6C). The *upd3-C-GFP* reporter was not detected in the larval midgut under basal conditions but, following *Ecc15* infection, was induced in old larval ECs, in agreement with the results of the *upd3-lacZ* reporter, with which it shares overlapping enhancer sequences (Houtz et al., 2017). The *upd3-R-GFP* reporter was also switched on by infection but appeared exclusively in AMP islets undergoing

(B and C) Venn Diagrams representing the number of genes found up or downregulated in response to infection in guts of larvae, adults, or both.

(D) Summary table of genes upregulated in response to larval gut infection and the pathways to which they belong. White shading indicates low induction; red shading indicates high induction.

(E–K) qPCR measurements of the expression of JAK-STAT (*upd2*, *upd3*, *Socs36E*), Notch (*Dl* and mβ), and Dpp (*dpp* and *Dad*) pathway genes in the guts of unchallenged and *Ecc15* infected, wildtype larvae at 4, 8, 12, 24, and 48 h post-treatment. Statistical significance: mean values of at least 3 repeats are represented ± SEM. *$p < 0.05$, **$p < 0.01$, ***$p < 0.001$ (Student's t test), comparing for each time point infected versus unchallenged.

See also Figure S4.

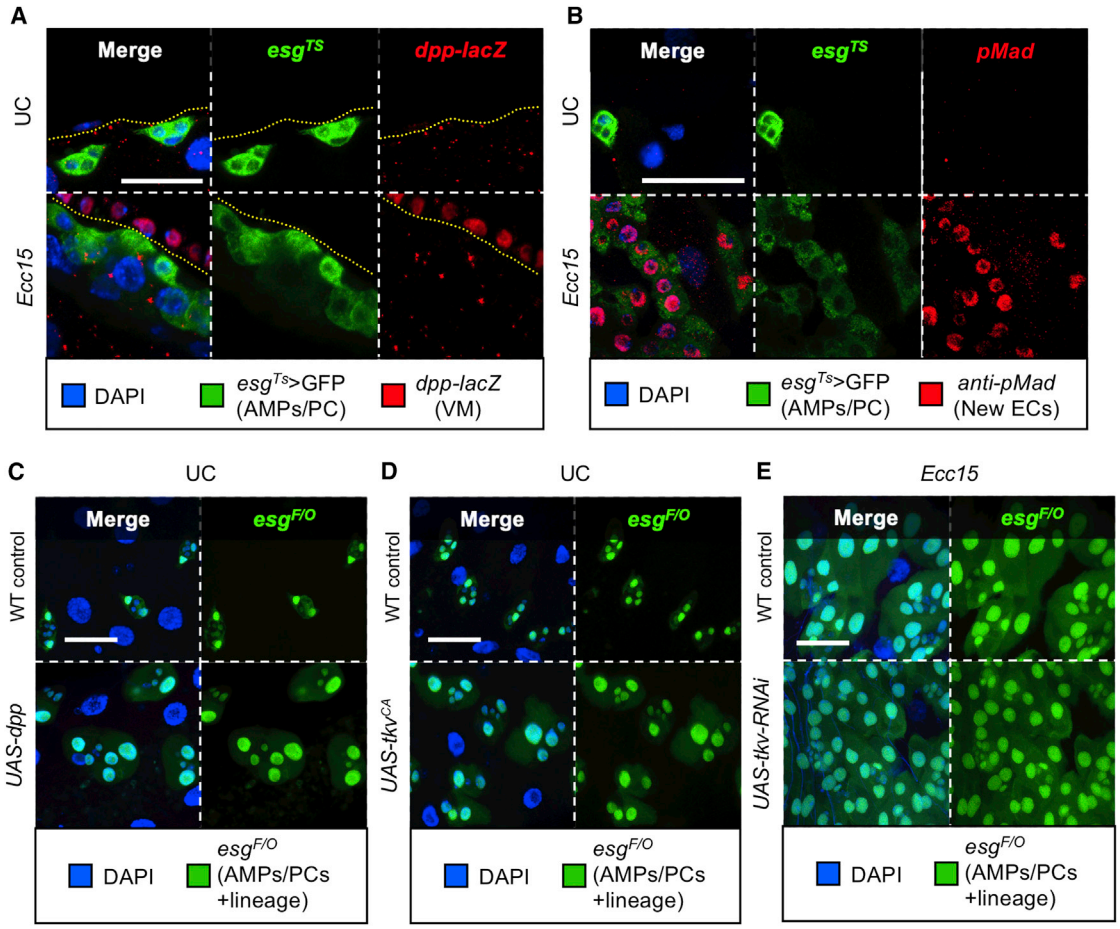

Figure 5. Dpp Pathway Activation Is Sufficient to Promote AMP Differentiation but Not Necessary in Response to Enteric Infection

(A and B) *Ecc15* infection stimulates *dpp* expression in visceral muscle, reported by *dpp-lacZ* (red) in cross-sectional midgut imaging (A) (yellow dotted line represents boundary between visceral muscle and midgut epithelia) and by Mad phosphorylation (anti-pMad, red) in differentiating AMPs (B). AMPs and newly differentiated ECs are marked in GFP (esg^{TS}, green).

(C and D) Ectopic activation of the Dpp pathway in AMPs ($esg^{F/O}$, green) by overexpression of the Dpp ligand (C) or a constitutively active form of the receptor, Tkv (D) induces differentiation of AMPs into new ECs.

(E) Blocking the Dpp pathway via AMP-specific ($esg^{F/O}$, green) RNAi knockdown of *tkv*, however, does not prevent AMP differentiation following *Ecc15* infection.

Images are representative of cells present in five or more guts per sample group in at least three replicates. Scale bars are 50 μm.

See also Figure S5.

differentiation. These results mirrored the adult gut, in which *upd3-C-GFP* reported infection-induced expression specifically in ECs while *upd3-R-GFP* was found to be activated in differentiating ISCs and EBs upon infectious damage. *Ecc15* infection also induced the expression of another major JAK-STAT cytokine, *upd2*, in ECs as well as AMPs (Figure 6C). Altogether, this demonstrates that infection triggers early induction of the JAK-STAT pathway in AMP islets, possibly via transcriptional activation of *upd2 and upd3*.

We next sought to determine if the JAK-STAT pathway regulates AMP differentiation during oral *Ecc15* larval infection. Blocking the JAK-STAT pathway by overexpressing an inhibitor of the JAK-STAT pathway, Latran, and a dominant-negative form of the JAK-STAT receptor Domeless ($esg^{F/O}$>*UAS-lat;UAS-Dome*^{DN}), had no effect on islets in UC conditions, but prevented AMP differentiation upon infection (Figure 6D). Similarly, RNAi knockdown of the JAK kinase, hop, strongly blocked AMP differentiation (Figure S6D). Activation of JAK-STAT by overexpressing Upd3 in AMP islets ($esg^{F/O}$>*UAS-upd3*) triggered the differentiation of islet cells into ECs (Figure 6E). In total, these results demonstrate that *Ecc15* infection activates the JAK-STAT pathway in the larval midgut via transcriptional upregulation of *upd3*, and that this activation is both required and sufficient to cause islet cells to differentiate into new ECs. Since the Notch and Dpp pathways were also found to be activated during infection and to play a role in AMP differentiation, we tested possible epistatic interactions between these pathways and JAK-STAT pathway by RT-qPCR (Figures S6E–S6K). As expected, *upd3* expression was eliminated in *upd3Δ* and *upd2-3Δ* mutants and upd2 expression only in upd2-*3Δ* mutants. *Socs36E* induction by infection was also only eliminated in *upd2-3Δ* double mutant flies, suggesting that *upd2* expression is sufficient to activate the JAK-STAT pathway during oral infection. Interestingly, *Dl* and *mβ* expression were strongly reduced

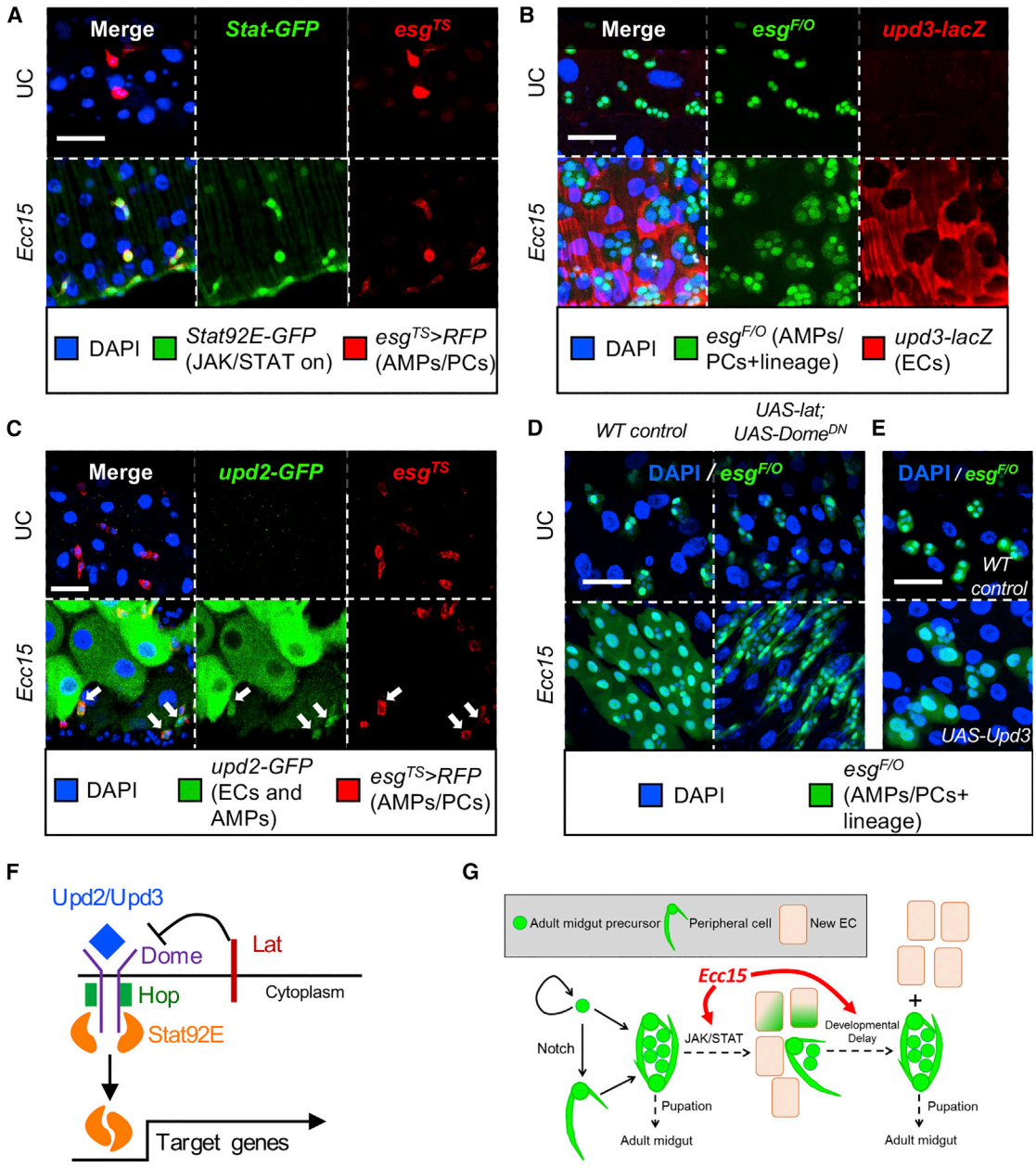

Figure 6. The JAK-STAT Pathway Is Activated by Bacterial Infection of the Larval Midgut and Is Both Necessary and Sufficient to Promote Tissue Repair via Differentiation of AMPs

(A) Stat92E (*10xStat-GFP*, green) is inactive in 2nd instar larval midguts, but is switched on in AMPs (esg^{TS}, red) and visceral muscles 4 h post-infection.

(B) *Upd3-lacZ* (red) is induced upon *Ecc15* infection in the larval ECs surrounding differentiating AMPs islets ($esg^{F/O}$, green).

(C) *upd2* expression (*upd2-GFP*, green) is induced in ECs and AMPs (esg^{TS}, red, arrows) of larval midguts by 6 h post-infection.

(D) Blocking the JAK-STAT pathway in AMP islets and their lineage ($esg^{F/O}$, green) by induced expression of *UAS-lat; UAS-DomeDN* has no effect in UC conditions but prevents AMPs from differentiating into polyploid ECs upon infection.

(E) Overexpression of the JAK-STAT ligand, Upd3, in AMPs and their lineage ($esg^{F/O}$, green) induces differentiation into new ECs.

(F) Cartoon of the JAK-STAT pathway.

(G) Model of AMP proliferation and differentiation in basal and bacterially challenged conditions. Nuclei are marked with DAPI (blue). Images are representative of cells present in five or more guts per sample group in at least three replicates. Scale bars: 50 μm for (A), (B), (D), and (E) and 25 μm for (C).

See also Figures S4 and S6.

in *upd2-3Δ* flies, implying that JAK-STAT acts upstream of the Notch pathway. In addition, transcription of *Dad*, was impaired in *upd2-3Δ* flies, but loss of JAK-STAT cytokines had no significant effect on *dpp* transcription upon infection. Overall, the JAK-STAT pathway is central to infection-induced differentiation and involved in regulating the Notch and Dpp pathways.

DISCUSSION

Unlike most epithelial tissues, such as the adult *Drosophila* midgut (Buchon et al., 2010; Duronio, 1999), the epithelium of the larval *Drosophila* midgut lacks progenitor cells to mediate constant turnover (Mathur et al., 2010), possibly due to the transient nature of larval tissues. Nevertheless, the larval midgut is exposed to environmental challenges such as ingested pathogenic microbes. In this manuscript, we asked how infection alters the developmental program of the *Drosophila* midgut, and how infectious damage is handled by tissue lacking resident stem cells. We found that, in response to infection with *Ecc15*, the larval midgut mounts limited tissue repair by transiently recruiting progenitors from imaginal structures. Specifically, ingestion of *Ecc15* triggers the expression of the *upd2* and *upd3* cytokines and activates the JAK-STAT pathway in visceral muscles and imaginal islet cells, resulting in the differentiation of progenitors into new ECs. This process transiently competes with AMP proliferation over the course of a developmental delay following infection. Our study gives insight into an alternative method of epithelial repair, in which imaginal adult midgut tissue is recruited for regeneration of the larval gut epithelium, controlled by the Notch, Dpp, and JAK-STAT pathways.

Limited Tissue Repair May Make Developing Organisms More Susceptible to Infection

While adult flies do not succumb to a wild-type *Ecc15* infection, or low doses of *P. entomophila* or *P. aeruginosa*, the high mortality caused by the same doses of bacteria in larvae highlights the constraints of an organism during its developmental stages. We speculate that one of the mechanisms underlying such differences is the ability to repair damaged tissue. While adults fully regenerate the midgut 48h post-infection by *Ecc15* (Buchon et al., 2010), the larval midgut never returns to its original size. Instead, limited tissue repair occurs and maintains the gut in a shortened state until the time of pupation. This incomplete regeneration could indicate two different scenarios. First, it is possible that gut repair in larvae is constrained to maintain a sufficient number of AMPs for the development of the adult midgut epithelium. Alternatively, it is possible that the number of AMPs present at the time of infection is a limiting factor, and is not enough to quickly buffer damage in dying larvae. Considering that most larvae (up to 60%) die from infection, and that limiting the number of AMPs using RNAi against EGFR resulted in an increase in susceptibility, we feel that the second model is more probable. Accordingly, it is possible that those that die during YP to BP transition failed to preserve the lower limit of AMPs necessary for metamorphosis. Moreover, increasing the dose of *Ecc15* leads to greater lethality, suggesting that larvae can only tolerate a fixed amount of damage. This result is counterintuitive, as developing organisms generally have higher reparative capability compared to adults (Tang et al., 2014; Yannas, 2005). This could be a particularity of insects that restrict cell proliferation to imaginal structures and achieve larval growth by polyploidization. Such a ''weakness'' in the tolerance to pathogens may also explain why most successful biocontrol strategies against insects target the larval stage (Vallet-Gely et al., 2008).

Developmental Delay Allows Recovery of the Pool of AMPs

One consequence of using the pool of imaginal cells to repair the larval midgut without increasing proliferation is the necessity of a lengthened larval growth period. Strikingly, when we measured the total number of AMPs in the guts of larvae that survived *Ecc15* ingestion and reached the wL3 stage, we found that the number was approximately equal to that of UC wL3 larvae. Guts of infected larvae had fewer islets, demonstrating that some imaginal structures are lost during tissue repair. However, the remaining islets contained more AMPs than in UC guts, thus preserving the total number at the wL3 stage between infected and UC guts. AMP reconstitution without an increase in proliferation requires a developmental delay for completion. We demonstrated that AMP renewal over the course of the delay is key for survival through metamorphosis. Developmental delays have previously been found to be critical for coordinating the repair of damaged imaginal structures (Halme et al., 2010; Hariharan and Serras, 2017; Smith-Bolton, 2016; Smith-Bolton et al., 2009). Our data present an example of such a delay that occurs as a consequence of larval epithelial damage, rather than damage to an imaginal structure. It is possible that other larval tissues can be repaired by imaginal cells, but to our knowledge, this has yet to be reported. Alternatively, this repair mechanism may be unique to the larval midgut, reflecting its important barrier and digestive functions.

The fact that developmental delay allows lost AMPs to be replenished to their normal number before pupation suggests that the quantity of AMPs is tightly controlled and crucial for metamorphosis success. However, although the delay is required for survival and recovery of AMP islets, it is not induced by the actual depletion of AMPs. Specifically, blocking AMP proliferation after infection did not slow or block the transition to the pupal stage, though it did lead to complete pupal lethality. It was proposed that the delay could result from food uptake blockage induced by infection (Keita et al., 2017). We found that feeding is resumed, at a reduced rate, a few hours after infection. It is possible that nutrient absorption in *Ecc15*-infected guts is affected, as the organ is severely shortened, and new ECs are smaller and display lower ploidy than ECs in UC guts. Accordingly, it was previously found that infection is associated with decreased expression of genes involved in protein digestion (Erkosar et al., 2015), and our transcriptome analysis confirms that digestive and metabolic functions are reduced (Figure S4D). Alternatively, signals similar to those secreted in response to imaginal disc damage may play a role in this delay. Indeed, our transcriptome analysis suggests that some key genes previously identified as regulating the insulin pathway, a key pathway to promote larval growth and development, are also regulated in the gut by infection, including *IMPL2* (Grewal, 2009; Kwon et al., 2015).

The Response to Infection in Adults and Larvae: One Network but Different Cell Responses

In this study, we identified a regenerative modality for systems devoid of dedicated stem cells. This response shows striking similarities and differences when compared with the adult midgut response. Parallel to the larval midgut, the adult *Drosophila* midgut is comprised of differentiated absorptive ECs and EEs. These differentiated cells are maintained through

a population of ISCs (Micchelli and Perrimon, 2006; Ohlstein and Spradling, 2007). ISCs give rise to either EEs through a pre-EE stage, or to ECs via partially differentiated enteroblasts (EBs) (Beehler-Evans and Micchelli, 2015; Zeng and Hou, 2015). EBs are poised for differentiation and become ECs when required (Antonello et al., 2015). This process has strong parallels with the larval midgut, and similar markers and pathways define epithelial cell lineages in both stages. We may consider AMPs as ISC equivalents of the larval gut. PCs, which act as differentiated progenitor cells and a niche for AMPs, can be viewed as cellular paralogs to EBs. Both EBs and PCs engage differentiation in response to damage (Buchon et al., 2009a). Despite these parallels, major differences exist between the two systems; for instance, there is neither basal turnover nor infection-induced proliferation in larvae. These disparities render the larval gut not truly "homeostatic," which has important consequences for larval survival following enteric damage.

Parallels in the genetic network controlling tissue repair can also be found. In both systems, the Notch and JAK-STAT pathways are essential for differentiation (Beebe et al., 2010; Ohlstein and Spradling, 2007; Perdigoto et al., 2011). While these pathways work in parallel for EC differentiation in adults (Zhai et al., 2017), their action seems uncoupled in larvae, allowing for the existence of a differentiated intermediate, the PC. Accordingly, in UC larvae, we detect JAK-STAT activation only starting in the late 3rd instar larvae stage, suggesting that infection triggers the premature transition of PCs into ECs that normally occurs in pupation. This raises the possibility that the repaired larval midgut is "patched" by pupal or adult-like ECs rather than by new larval ECs. The lower ploidy of the ECs generated upon infection of the larval midgut agrees with this hypothesis. This contrasts with the response of the adult midgut to infection, which triggers the generation of ECs with higher ploidy than their UC counterparts (Xiang et al., 2017). In the adult midgut, the TGF-β/Dpp pathway regulates multiple aspects of epithelial maintenance, including ISC self-renewal and quiescence, EC differentiation, and *upd3* expression in ECs (Guo et al., 2013; Houtz et al., 2017; Li et al., 2013a, 2013b; Zhou et al., 2015). While previous studies have shown that Dpp signaling prevents the differentiation of AMPs in larvae, suggesting a contrast in roles between adults and larvae (Mathur et al., 2010), we surprisingly found that ectopic activation of Dpp signaling in AMPs induced their differentiation. It is possible that this was the result of a neomorphic effect due to protein overexpression. However, inhibiting the Dpp pathway in AMPs neither promoted nor completely blocked AMP differentiation, suggesting that it may contribute, secondarily, to progenitor differentiation rather than inhibiting it. We found that the JAK-STAT pathway regulates infection-induced AMP differentiation. The induction of the JAK-STAT pathway upon infection is controlled in both adult and larval midguts by the transcriptional activation of the Upd2 and Upd3 cytokines in ECs (Houtz et al., 2017; Osman et al., 2012). Strikingly, we found that similar enhancers are used to induce *upd3* expression in both systems, also suggesting a common sensing mechanism.

Conclusions

Altogether, our results demonstrate that, while the cellular bases and molecular mechanisms underlying tissue repair in adults and larvae are largely similar, specific differences result in a dramatically dissimilar outcome to infection. This implies that precise developmental cues, possibly hormonal regulation, alters tissue repair mechanisms with important consequences for health. In addition, our results also illustrate how the constraints of development can sensitize hosts to stresses such as infection. The apparent trade-off between the constraints of development and the impact of environmental stresses, such as infection, could be conserved and suggest that adult and immature intestinal homeostasis could differ in mammals as well. Finally, our data suggest that limited homeostatic abilities at the larval stage could explain why larvae are more susceptible to biocontrol strategies.

STAR★METHODS

Detailed methods are provided in the online version of this paper and include the following:

- KEY RESOURCES TABLE
- LEAD CONTACT AND MATERIALS AVAILABILITY
- EXPERIMENTAL MODEL DETAILS
  - Fly Stocks and Husbandry
- METHOD DETAILS
  - Bacterial Oral Infection
  - Survival and Development Rate Experiments
  - Feeding Rate Experiments
  - Immunohistochemistry and Fluorescence Imaging
  - Estimation of Total Midgut AMPs
  - Transcriptome Analysis
  - RT-qPCR
  - MARCM Clones
- QUANTIFICATION AND STATISTICAL ANALYSIS
- DATA AND CODE AVAILABILITY

SUPPLEMENTAL INFORMATION

Supplemental Information can be found online at https://doi.org/10.1016/j.chom.2019.08.006.

ACKNOWLEDGMENTS

We would like to thank Jonathan Revah for his exploratory experiments that contributed to this project. In addition, we thank Jeff Hodgson, Peter Nagy, and Bretta Hixson for comments on the manuscript. This work was supported by NSF IOS1656118 and NSF IOS1653021 to N.B.

AUTHOR CONTRIBUTIONS

Conceptualization, P.H. and N.B.; Methodology and Investigation, P.H., A.B., and X.B.; Software, X.B.; Formal Analysis, P.H., X.B., and N.B.; Writing (Original & Review) and Visualization, P.H., A.B., and N.B.; Validation, Resources, Project Administration, Funding Acquisition, and Supervision, N.B.

DECLARATION OF INTERESTS

The authors declare no competing interests.

Received: September 21, 2018
Revised: June 11, 2019
Accepted: August 6, 2019
Published: September 3, 2019

REFERENCES

Acosta Muniz, C., Jaillard, D., Lemaitre, B., and Boccard, F. (2007). Erwinia carotovora Evf antagonizes the elimination of bacteria in the gut of Drosophila larvae. Cell. Microbiol. *9*, 106–119.

Antonello, Z.A., Reiff, T., Ballesta-Illan, E., and Dominguez, M. (2015). Robust intestinal homeostasis relies on cellular plasticity in enteroblasts mediated by miR-8-Escargot switch. EMBO J. *34*, 2025–2041.

Bach, E., Ekas, L., Ayala-Camargo, A., Flaherty, M.S., Lee, H., Perrimon, N., and Baeg, G.-H. (2007). GFP reporters detect the activation of the Drosophila JAK/STAT pathway in vivo. Gene Expr. Patterns *7*, 323–331.

Bae, Y.S., Choi, M.K., and Lee, W.J. (2010). Dual oxidase in mucosal immunity and host-microbe homeostasis. Trends Immunol. *31*, 278–287.

Basset, A., Tzou, P., Lemaitre, B., and Boccard, F. (2003). A single gene that promotes interaction of a phytopathogenic bacterium with its insect vector, Drosophila melanogaster. EMBO Rep. *4*, 205–209.

Beebe, K., Lee, W.C., and Micchelli, C.A. (2010). JAK/STAT signaling coordinates stem cell proliferation and multilineage differentiation in the Drosophila intestinal stem cell lineage. Dev. Biol. *338*, 28–37.

Beehler-Evans, R., and Micchelli, C.A. (2015). Generation of enteroendocrine cell diversity in midgut stem cell lineages. Development *142*, 654–664.

Bhatt, P.K., and Neckameyer, W.S. (2013). Functional analysis of the larval feeding circuit in Drosophila. J. Vis. Exp. *81*, e51062.

Bonfini, A., Liu, X., and Buchon, N. (2016). From pathogens to microbiota: how Drosophila intestinal stem cells react to gut microbes. Dev. Comp. Immunol. *64*, 22–38.

Buchon, N., Broderick, N.A., Chakrabarti, S., and Lemaitre, B. (2009a). Invasive and indigenous microbiota impact intestinal stem cell activity through multiple pathways in Drosophila. Genes Dev. *23*, 2333–2344.

Buchon, N., Broderick, N.A., Poidevin, M., Pradervand, S., and Lemaitre, B. (2009b). Drosophila intestinal response to bacterial infection: activation of host defense and stem cell proliferation. Cell Host Microbe *5*, 200–211.

Buchon, N., Broderick, N.A., Kuraishi, T., and Lemaitre, B. (2010). Drosophila EGFR pathway coordinates stem cell proliferation and gut remodeling following infection. BMC Biol. *8*, 152.

Buchon, N., Broderick, N.A., and Lemaitre, B. (2013). Gut homeostasis in a microbial world: insights from Drosophila melanogaster. Nat. Rev. Microbiol. *11*, 615–626.

Buchon, N., Silverman, N., and Cherry, S. (2014). Immunity in Drosophila melanogaster - from microbial recognition to whole-organism physiology. Nat. Rev. Immunol. *14*, 796–810.

Colombani, J., Andersen, D.S., and Léopold, P. (2012). Secreted peptide Dilp8 coordinates Drosophila tissue growth with developmental timing. Science *336*, 582–585.

Denton, D., Shravage, B., Simin, R., Mills, K., Berry, D.L., Baehrecke, E.H., and Kumar, S. (2009). Autophagy, not apoptosis, is essential for midgut cell death in Drosophila. Curr. Biol. *19*, 1741–1746.

Dobin, A., Davis, C., Schlesinger, F., Drenkow, J., Zaleski, C., Jha, S., Batut, P., Chaisson, M., and Gingeras, T. (2013). STAR: ultrafast universal RNA-seq aligner. Bioinformatics *29*, 15–21.

Du, E.J., Ahn, T.J., Kwon, I., Lee, J.H., Park, J.H., Park, S.H., Kang, T.M., Cho, H., Kim, T.J., Kim, H.W., et al. (2016). TrpA1 regulates defecation of food-borne pathogens under the control of the Duox pathway. PLoS Genet. *12*, e1005773.

Duronio, R.J. (1999). Establishing links between developmental signaling pathways and cell-cycle regulation in Drosophila. Curr. Opin. Genet. Dev. *9*, 81–88.

Erkosar, B., Storelli, G., Mitchell, M., Bozonnet, L., Bozonnet, N., and Leulier, F. (2015). Pathogen virulence impedes mutualist-mediated enhancement of host juvenile growth via inhibition of protein digestion. Cell Host Microbe *18*, 445–455.

Evans, C.J., Olson, J.M., Ngo, K.T., Kim, E., Lee, N.E., Kuoy, E., Patananan, A.N., Sitz, D., Tran, P., Do, M.T., et al. (2009). G-TRACE: rapid Gal4-based cell lineage analysis in Drosophila. Nat. Methods *6*, 603–605.

Furriols, M., and Bray, S. (2001). A model Notch response element detects suppressor of hairless-dependent molecular switch. Curr. Biol. *11*, 60–64.

Grewal, S.S. (2009). Insulin/TOR signaling in growth and homeostasis: a view from the fly world. Int. J. Biochem. Cell Biol. *41*, 1006–1010.

Guo, Z., Driver, I., and Ohlstein, B. (2013). Injury-induced BMP signaling negatively regulates Drosophila midgut homeostasis. J. Cell Biol. *201*, 945–961.

Halme, A., Cheng, M., and Hariharan, I.K. (2010). Retinoids regulate a developmental checkpoint for tissue regeneration in Drosophila. Curr. Biol. *20*, 458–463.

Hariharan, I.K., and Serras, F. (2017). Imaginal disc regeneration takes flight. Curr. Opin. Cell Biol. *48*, 10–16.

Houtz, P., Bonfini, A., Liu, X., Revah, J., Guillou, A., Poidevin, M., Hens, K., Huang, H.Y., Deplancke, B., Tsai, Y.C., et al. (2017). Hippo, TGF-β, and Src-MAPK pathways regulate transcription of the upd3 cytokine in Drosophila enterocytes upon bacterial infection. PLoS Genet. *13*, e1007091.

Houtz, P.L., and Buchon, N. (2014). Methods to assess intestinal stem cell activity in response to microbes in Drosophila melanogaster. Methods Mol. Biol. *1213*, 171–182.

Hu, Y., Sopko, R., Foos, M., Kelley, C., Flockhart, I., Ammeux, N., Wang, X., Perkins, L., Perrimon, N., and Mohr, S.E. (2013). FlyPrimerBank: an online database for Drosophila melanogaster gene expression analysis and knockdown evaluation of RNAi reagents. G3 (Bethesda) *3*, 1607–1616.

Jaszczak, J.S., Wolpe, J.B., Bhandari, R., Jaszczak, R.G., and Halme, A. (2016). Growth coordination during Drosophila melanogaster imaginal disc regeneration is mediated by signaling through the relaxin receptor Lgr3 in the prothoracic gland. Genetics *204*, 703–709.

Jiang, H., and Edgar, B.A. (2009). EGFR signaling regulates the proliferation of Drosophila adult midgut progenitors. Development *136*, 483–493.

Jiang, H., Patel, P.H., Kohlmaier, A., Grenley, M.O., Mcewen, D.G., and Edgar, B.A. (2009). Cytokine/Jak/Stat signaling mediates regeneration and homeostasis in the Drosophila midgut. Cell *137*, 1343–1355.

Jiang, H., Grenley, M.O., Bravo, M.J., Blumhagen, R.Z., and Edgar, B.A. (2011). EGFR/Ras/MAPK signaling mediates adult midgut epithelial homeostasis and regeneration in Drosophila. Cell Stem Cell *8*, 84–95.

Karin, M., and Clevers, H. (2016). Reparative inflammation takes charge of tissue regeneration. Nature *529*, 307–315.

Karpowicz, P., Perez, J., and Perrimon, N. (2010). The Hippo tumor suppressor pathway regulates intestinal stem cell regeneration. Development *137*, 4135–4145.

Keita, S., Masuzzo, A., Royet, J., and Kurz, C.L. (2017). Drosophila larvae food intake cessation following exposure to Erwinia contaminated media requires odor perception, Trpa1 channel and evf virulence factor. J. Insect Physiol. *99*, 25–32.

Kwon, Y., Song, W., Droujinine, I.A., Hu, Y., Asara, J.M., and Perrimon, N. (2015). Systemic organ wasting induced by localized expression of the secreted insulin/IGF antagonist ImpL2. Dev. Cell *33*, 36–46.

Lee, T., and Luo, L. (2001). Mosaic analysis with a repressible cell marker (MARCM) for Drosophila neural development. Trends Neurosci. *24*, 251–254.

Lemaitre, B., and Hoffmann, J.A. (2007). The host defense of Drosophila melanogaster. Annu. Rev. Immunol. *25*, 697–743.

Li, H., Qi, Y., and Jasper, H. (2013a). Dpp signaling determines regional stem cell identity in the regenerating adult Drosophila gastrointestinal tract. Cell Rep. *4*, 10–18.

Li, Z., Zhang, Y., Han, L., Shi, L., and Lin, X. (2013b). Trachea-derived dpp controls adult midgut homeostasis in Drosophila. Dev. Cell *24*, 133–143.

Liu, X., Hodgson, J.J., and Buchon, N. (2017). Drosophila as a model for homeostatic, antibacterial, and antiviral mechanisms in the gut. PLoS Pathog. *13*, e1006277.

Makki, R., Meister, M., Pennetier, D., Ubeda, J.-M., Braun, A., Daburon, V., Joanna, K., Bourbon, H.-M., Zhou, R., Vincent, A., and Crozatier, M. (2010). A Short Receptor Downregulates JAK/STAT Signalling to Control the Drosophila Cellular Immune Response *8*, https://doi.org/10.1371/journal.pbio.1000441.

Mathur, D., Bost, A., Driver, I., and Ohlstein, B. (2010). A transient niche regulates the specification of Drosophila intestinal stem cells. Science *327*, 210–213.

Micchelli, C.A., and Perrimon, N. (2006). Evidence that stem cells reside in the adult Drosophila midgut epithelium. Nature *439*, 475–479.

Micchelli, C.A., Sudmeier, L., Perrimon, N., Tang, S., and Beehler-Evans, R. (2011). Identification of adult midgut precursors in Drosophila. Gene Expr. Patterns *11*, 12–21.

Nagy, P., Sándor, G.O., and Juhász, G. (2018). Autophagy maintains stem cells and intestinal homeostasis in Drosophila. Sci. Rep. *8*, 4644.

Ohlstein, B., and Spradling, A.C. (2007). Multipotent Drosophila intestinal stem cells specify daughter cell fates by differential notch signaling. Science *315*, 988–992.

Osman, D., Buchon, N., Chakrabarti, S., Huang, Y.-T., Su, W.-C., Poidevin, M., Tsai, Y.-C., and Lemaitre, B. (2012). Autocrine and paracrine unpaired signaling regulate intestinal stem cell maintenance and division. J. Cell Sci. *125*, 5944–5949.

Perdigoto, C.N., Schweisguth, F., and Bardin, A.J. (2011). Distinct levels of Notch activity for commitment and terminal differentiation of stem cells in the adult fly intestine. Development *138*, 4585–4595.

Schindelin, J., Arganda-Carreras, I., Frise, E., Kaynig, V., Longair, M., Pietzsch, T., Preibisch, S., Rueden, C., Saalfeld, S., Schmid, B., Tinevez, J.-Y., White, D.J., Hartenstein, V., Eliceiri, K., Tomancak, P., and Cardona, A. (2012). Fiji: an open-source platform for biological-image analysis. Nat. Methods *9*, 676–682.

Smith-Bolton, R. (2016). Drosophila imaginal discs as a model of epithelial wound repair and regeneration. Adv. Wound Care (New Rochelle) *5*, 251–261.

Smith-Bolton, R.K., Worley, M.I., Kanda, H., and Hariharan, I.K. (2009). Regenerative growth in Drosophila imaginal discs is regulated by Wingless and Myc. Dev. Cell *16*, 797–809.

Soldano, A., Alpizar, Y.A., Boonen, B., Franco, L., López-Requena, A., Liu, G., Mora, N., Yaksi, E., Voets, T., Vennekens, R., et al. (2016). Gustatory-mediated avoidance of bacterial lipopolysaccharides via TRPA1 activation in Drosophila. eLife *5*.

Stensmyr, M.C., Dweck, H.K.M., Farhan, A., Ibba, I., Strutz, A., Mukunda, L., Linz, J., Grabe, V., Steck, K., Lavista-Llanos, S., et al. (2012). A conserved dedicated olfactory circuit for detecting harmful microbes in Drosophila. Cell *151*, 1345–1357.

Tang, Q.-M., Chen, J.L., Shen, W.L., Yin, Z., Liu, H.H., Fang, Z., Heng, B.C., Ouyang, H.W., and Chen, X. (2014). Fetal and adult fibroblasts display intrinsic differences in tendon tissue engineering and regeneration. Sci. Rep. *4*, 5515.

Troha, K., and Buchon, N. (2019). Methods for the study of innate immunity in Drosophila melanogaster. Wiley Interdiscip. Rev. Dev. Biol. e344.

Vallet-Gely, I., Lemaitre, B., and Boccard, F. (2008). Bacterial strategies to overcome insect defences. Nat. Rev. Microbiol. *6*, 302–313.

Xiang, J., Bandura, J., Zhang, P., Jin, Y., Reuter, H., and Edgar, B.A. (2017). EGFR-dependent TOR-independent endocycles support Drosophila gut epithelial regeneration. Nat. Commun. *8*, 15125.

Yannas, I.V. (2005). Similarities and differences between induced organ regeneration in adults and early foetal regeneration. J. R. Soc. Interface *2*, 403–417.

Zeng, X., Chauhan, C., and Hou, S.X. (2010). Characterization of midgut stem cell- and enteroblast-specific Gal4 lines in Drosophila. Genesis *48*, 607–611.

Zeng, X., and Hou, S.X. (2015). Enteroendocrine cells are generated from stem cells through a distinct progenitor in the adult Drosophila posterior midgut. Development *142*, 644–653.

Zhai, Z., Boquete, J.P., and Lemaitre, B. (2017). A genetic framework controlling the differentiation of intestinal stem cells during regeneration in Drosophila. PLoS Genet. *13*, e1006854.

Zhai, Z., Boquete, J.P., and Lemaitre, B. (2018). Cell-specific Imd-NF-κB responses enable simultaneous antibacterial immunity and intestinal epithelial cell shedding upon bacterial infection. Immunity *48*, 897–910.

Zhou, J., Florescu, S., Boettcher, A.L., Luo, L., Dutta, D., Kerr, G., Cai, Y., Edgar, B.A., and Boutros, M. (2015). Dpp/Gbb signaling is required for normal intestinal regeneration during infection. Dev. Biol. *399*, 189–203.

STAR★METHODS

KEY RESOURCES TABLE

REAGENT or RESOURCE	SOURCE	IDENTIFIER
Antibodies		
rabbit anti-pH3	Millipore	Cat# 06-570, RRID:AB_310177
rabbit anti-β-Galactosidase	MP Biomedicals	Cat# 0855976, RRID:AB_2334934
goat anti-β-Galactosidase	MP Biomedicals	Cat#0856028
mouse anti-Prospero	DHSB	Cat# Prospero (MR1A), RRID: AB_528440
mouse anti-Delta	DSHB	Cat# c594.9b, RRID:AB_528194
donkey anti-rabbit-555	Thermo Fisher Scientific	Cat# A-31572, RRID:AB_162543
donkey anti-goat-555	Thermo Fisher Scientific	Cat# A-21432, RRID:AB_2535853
donkey anti-mouse-488	Thermo Fisher Scientific	Cat# A-21202, RRID:AB_141607
donkey anti-mouse-647	Thermo Fisher Scientific	Cat# A-31571, RRID:AB_162542
Rabbit anti Phospho-Smad1/5 (Ser463/465) (41D10)	Cell signaling Technology	Cat# 9516, RRID: AB_491015
Chicken anti GFP	Invitrogen	Cat# A10262, RRID: AB_2534023
Rabbit anti RFP	Invitrogen	Cat# R10367
Goat Anti-Chicken IgG (H+L) Antibody, Alexa Fluor 488 Conjugated	Invitrogen	Cat# A A11039, RRID: AB_142924
Bacterial and Virus Strains		
Erwinia carotovora ssp. carotovora 15	Basset et al., 2003	N/A
Erwinia carotovora ssp. carotovora 15 pOM evf	Basset et al., 2003	N/A
Chemicals, Peptides, and Recombinant Proteins		
FD&C Blue #1 dye	Spectrum Chemical	FD110
Critical Commercial Assays		
QuantSeq 3′ mRNA-Seq Library Prep Kit	Lexogen	SKU: 015.96
Deposited Data		
RNA-seq of adult and larval midguts with and without *Ecc15* infection	NCBI BioProject	PRJNA553080
Experimental Models: Organisms/Strains		
Dmel/Canton-S (Cs)	Bloomington	RRID: BDSC_64349
Dmel/Su(H)TS (w; Su(H)-Gal4, UAS-CD8-GFP/CyO; tubGal80TS/TM6C)	Zeng et al., 2010	N/A
Dmel/Su(H)-lacZ (Su(H)GBE-lacZ)	Furriols and Bray, 2001	N/A
Dmel/Myo-lacZ (Yw; pLacW Myo-lacZ/CyO)	Jiang et al., 2009	N/A
Dmel/MyoTS (w; Myo1A-Gal4, UAS-GFP, Tub-Gal80TS)	Jiang et al., 2009	N/A
Dmel/TkvRNAi (y[1] sc[*] v[1]; P{y[+t7.7] v[+t1.8] = TRiP.HMS04510}attP40)	Bloomington	RRID: BDSC_57309
Dmel/UAS-Upd3 (w;UAS-Upd3/CyO)	Buchon et al., 2009a	N/A
Dmel/UAS-lat;UAS-DomeDN (UAS-Latran; UAS-domeΔCYT3-2)	Makki et al., 2010	N/A
Dmel/upd3-lacZ (Upd3.1-lacZ)	Jiang et al., 2011	N/A
Dmel/UAS-RasV12 (w[1118]; P{w[+mC] = UAS-Ras85D.V12}TL1)	Bloomington	RRID: BDSC_4847
Dmel/UAS-dpp (w[*]; P{w[+mC] = UAS-dpp.S}42B.4)	Bloomington	RRID: BDSC_1486

(*Continued on next page*)

Continued

REAGENT or RESOURCE	SOURCE	IDENTIFIER
Dmel/UAS-TkvCA (w[*]; P{w[+mC] = UAS-tkv.Ca}3)	Bloomington	RRID: BDSC_36537
Dmel/esgTS mcherry (w^-;esg-Gal4,UAS-mcherry cd8, tubGal80TS/CyO)	Peter Nagy	N/A
Dmel/esgTS GFP (w; esg-Gal4, Tub-Gal80TS)	Jiang et al., 2009	N/A
Dmel/esgF/O (w; esg-Gal4, tub-Gal80TS, UAS-GFP; UAS-FLP tub_{FRT} $CD2_{FRT}$Gal4 UAS-GFP)	Jiang et al., 2011	N/A
Dmel/UAS-F/O (w^-,tubGal80ts; act-Gal4 UAS-FLP/TM2)	Jiang et al., 2011	N/A
Dmel/UAS-G-TRACE (w[*]; P{w[+mC] = UAS-RedStinger}4, P{w[+mC] = UAS-FLP.D}JD1, P{w[+mC] = Ubi-p63E(FRT.STOP)Stinger}9F6/CyO)	Bloomington	RRID: BDSC_28280
Dmel/esgTS Black (w; esgGal4 Gal8oTS/CyOtwiGFP)	Recombined in the lab using esg^{TS} as the base	this lab
Dmel/UAS-Nintra (y,w, hs-flp; UAS-N-Intra/CyO; MKRS/TM2)	Bloomington	RRID: BDSC_52008
Dmel/UAS-N-RNAi (y[1] v[1]; P{y[+t7.7] v[+t1.8] = TRiP.HMS00001}attP2)	Bloomington	RRID: BDSC_33611
Dmel/10xStat92eGFP N/A	Bach et al., 2007	N/A
Dmel/UAS-EGFR-RNAi (y[1] v[1]; P{y[+t7.7] v[+t1.8] = TRiP.HMS05003}attP40)	Bloomington	RRID: BDSC_60012
Dmel/Upd3-C-GFP	Houtz et al., 2017	this lab
Dmel/Upd3-R-GFP	Houtz et al., 2017	this lab
Dmel/NRE-GFP (w[1118]; P{w[+m*] = NRE-EGFP.S}5A)	Bloomington	RRID: BDSC_30727
Dmel/UAS-Mad-RNAi (y[1] sc[*] v[1] sev[21]; P{y[+t7.7]v[+t1.8] = TRiP.GL01527}attP40)	Bloomington	RRID: BDSC_43183
Dmel/UAS-put-RNAi (y[1] sc[*] v[1] sev[21]; P{y[+t7.7] v[+t1.8] = TRiP.HMS01944}attP40)	Bloomington	RRID: BDSC_39025
Dmel/UAS-hop-RNAi (y[1] sc[*] v[1] sev[21]; P{y[+t7.7] v[+t1.8] = TRiP.HMS00761}attP2)	Bloomington	RRID: BDSC_32966
Dmel/tkv^4 FRT40A (w[*]; tkv[4] P{ry[+t7.2] = neoFRT}40A/CyO)	Bloomington	RRID: BDSC_58786
Dmel/MARCM hsFlp, Tub-Gal4, UAS-GFP/FM7; Tub-Gal80, FRT40A/CyO	Karpowicz et al., 2010	Dr. Norbert Perrimon
Dmel/FRT40A Control (y[1] w[1118]; P{w[+mC] = Ubi-mRFP.nls}2L P{ry[+t7.2] = neoFRT}40A/CyO)	Bloomington	RRID: BDSC_34500
Dmel/upd2CBGFP (w; upd2_CB-GFP.attP40)	Zhai et al., 2018	Dr. Bruno Lemaitre
Dmel/ esgTS RFP Esg-Gal4,tub-Gal80TS,UAS-mcherry-CD8	Nagy et al., 2018	Dr. Peter Nagy
Dmel/ dpp-Lacz 68153 (w[*]; P{w[+mC] = dpp-lacZ.P4}2/CyO)	Bloomington	RRID: BDSC_68153
Dmel/DITS GFP (w; Tub-Gal80TS, UAS-GFP/Cyo; Delta-Gal4/TM6C)	Zeng et al., 2010	Dr. Bruce Edgar
Dmel/ upd3[Delta] (w[*] upd3[Delta])	Bloomington	RRID: BDSC_55728
Dmel/upd2[Delta] upd3[Delta] (w[*] upd2[Delta] upd3[Delta])	Bloomington	RRID: BDSC_55729

(*Continued on next page*)

Continued

REAGENT or RESOURCE	SOURCE	IDENTIFIER
Oligonucleotides		
Primer: upd3_Fw: AGCCGGAGCGGTAACAAAA	Hu et al., 2013	N/A
Primer: upd3_Rv: CGAGTAAGATCAGTGACCAGTTC	Hu et al., 2013	N/A
Primer: upd2_Fw: TTCTCCGGCAAATCAGAGATCC	Hu et al., 2013	N/A
Primer: upd2_Rv: GCGCTTGATAACTCGTCCTTG	Hu et al., 2013	N/A
Primer: Socs36E_Fw: GCACAGAAGGCAGACC	Generated in the lab	N/A
Primer: Socs36E_Rv: ACGTAGGAGACCCGTAT	Generated in the lab	N/A
Primer: Delta_Fw: AATCCCATCCAGTTCCCCTTC	Hu et al., 2013	N/A
Primer: Delta_Rv: ATTGCCGCTGTTGTTCGTATC	Hu et al., 2013	N/A
Primer: dpp_Fw: TGGCGACTTTTCAAACGATTGT	Hu et al., 2013	N/A
Primer: dpp_Rv: CAGCGGAATATGAGCGGCAA	Hu et al., 2013	N/A
Primer: Dad_Fw: GAGTGTGCAAAGTGATGC	Hu et al., 2013	N/A
Primer: Dad_Rv: CTCATGCTCAGAAGTTCAGCCCTA	Hu et al., 2013	N/A
Primer: Rp49_Fw: GACGCTTCAAGGGACAGTATCTG	Generated in the lab	N/A
Primer: RP49_Rv: AAACGCGGTTCTGGATGAG	Generated in the lab	N/A
Software and Algorithms		
Fastqc	Babraham bioinformatics	https://www.bioinformatics.babraham.ac.uk/projects/fastqc/
Trimmomatic	Usadel Lab	http://www.usadellab.org/cms/?page=trimmomatic
STAR	Dobin et al., 2013	N/A
DEseq2	https://doi.org/10.18129/B9.bioc.DESeq2	https://bioconductor.org/packages/release/bioc/html/DESeq2.html
GraphPad Prism V7.0A For Mac OSX	GraphPad Software	www.graphpad.com
Microsoft Excel for Mac Ver. 15.27	Microsoft Corporation	N/A
Microsoft Word for Mac Ver. 15.27	Microsoft Corporation	N/A
ImageJ Ver. 2.0.0-rc-68/1.52e	Schindelin et al., 2012, Imagej.net	https://fiji.sc/

LEAD CONTACT AND MATERIALS AVAILABILITY

Further information and requests for resources and reagents should be directed to and will be fulfilled by the Lead Contact, Nicolas Buchon (nicolas.buchon@cornell.edu).

EXPERIMENTAL MODEL DETAILS

Fly Stocks and Husbandry

Drosophila stocks were maintained at room temperature (~23°C) on standard fly medium (sucrose, cornmeal, yeast, and agar). Control lines: as controls during Gal4-UAS experiments, we used the F1 progeny of the driver line crossed to wildtype stocks such as canton-S (Cs) (RRID: BDSC_64349). Gal4 Drivers: *Myo1A-Gal4, UAS-GFP, tub-Gal80^{TS}; upd3-lacZ* (*Myo^{TS}*, EC-specific), *Su(H) GBE-Gal4; UAS-GFP, tub-Gal80^{TS}* (*Su(H)^{TS}*, EB-specific), *esg-Gal4; UAS-GFP, tub-Gal80^{TS}* (*esg^{TS}*, adult midgut progenitor-specific) as well as *esg-Gal4, UAS-mcherry, tub-Gal80^{TS}*. Conditional *Gal4^{TS}* flies were obtained by crossing virgin females of the driver strain with males of the *UAS-transgene* line. For RNAi and overexpression experiments, F1 larvae (*driver > UAS-transgene*) were raised to 1st instars at 18°C, to allow for normal development up to this stage. Larvae were then switched to 29°C for 2-3days to allow for maximum transgene expression and RNAi-mediated gene knockdown. By this time, larvae were in 2nd and 3rd instar stages. UAS-transgene stocks: Transgenic fly lines were obtained from Bloomington (TriP lines), VDRC (Vienna) or NIG (Japan). Reporter lines: *upd3.1-lacZ*, *esg-lacZ, Myo-lacZ*. A list of the fly lines used in this report can be found in the Key Resources Table.

METHOD DETAILS

Bacterial Oral Infection

Erwinia carotovora ssp. Carotovora 15 (*Ecc15*) is a Gram-negative plant and insect pathogen, which is semi-lethal when ingested by *Drosophila* larvae, and nonlethal to adult flies (Troha and Buchon, 2019). The pathogenicity of *Ecc15* in insects is mediated by the

Erwinia virulence factor (Evf). Strains of *Ecc15* mutant for the *evf* gene (*Ecc15 evf*) or overexpressing it (*Ecc15 pOM evf*) were also used. Additional bacteria tested for comparative pathogenicity in larvae and adults include *Pseudomonas entomophila*, *Pseudomonas aeruginosa*, and *Providencia rettgeri*. All bacteria were maintained on standard LB agar plates. Bacteria were cultured in LB broth at 29°C for 16 h. Oral infection of larvae was performed as previously described (Acosta Muniz et al., 2007): larvae were collected from standard fly medium in 1X PBS and selected by stage (determined by observation of mouth hook and spiracle development), then moved to 1.5ml tubes containing 400μl of crushed, organic banana and 200μl of either 1X PBS solution (control) or a bacterial pellet solution, at OD_{600} = 100 concentration (for a final OD_{600} of 33) unless otherwise noted. Orally treated larvae were incubated at 29°C for 30 min before being transferred to fresh vials of standard fly medium, along with the contents of the 1.5ml incubation tubes. Infected larvae were then incubated at 29°C until dissection or for the duration of survival experiments. Oral infection of adult flies was performed as previously described (Houtz and Buchon, 2014): flies were starved for 2 h in empty vials at 29°C, and subsequently moved to fly medium vials, in which the food was covered by a filter paper disk containing 150μl of either 2.5% sucrose solution (UC control), or 5% sucrose solution mixed with an equal volume of a OD_{600} = 200 bacterial pellet unless noted otherwise. Orally treated flies were incubated at 29°C until dissection or for the duration of survival experiments. High doses of bacteria are used in the case of both adult and larval oral infections, in comparison to systemic infections, as they mimic natural infections of *Drosophila melanogaster* that can occur while feeding directly on bacterial biofilm found at the surface of rotting fruits (Buchon et al., 2013).

Survival and Development Rate Experiments

Larvae were grown at 29°C for two days after egg deposition (AED) and 2nd instar larvae were collected for treatment. For temperature inducible experiments, flies were allowed to hatch and develop to first instars at 18°C before shifting to 29°C. Following treatment, flies were monitored at 29°C each day and the number of flies that had reached the yellow pupa (YP), black pupa (BP), or adult stages was recorded. Emerged adults were collected from these experiments, when appropriate, and maintained at 29°C to monitor their survival. For adult survival following infection, 20 female flies aged 3days post-eclosion were collected for each treatment group and shifted to 29°C upon infection. Their survival was monitored daily, with the date of infection marked as day zero.

Feeding Rate Experiments

To measure the general amount of feeding, second instar larvae were treated as usual with either 1× PBS, or a bacterial pellet of wildtype or *evf* mutant *Ecc15* at a final concentration of OD_{600} = 66. Following treatment, larvae were transferred to vials of fly medium supplemented with 2% FD&C Blue #1 dye (Spectrum Chemical). Larvae were collected in 1X PBS each hour for 4 h and checked under a microscope for the presence of blue food in the gut. Mouth hook contractions per minute were recorded as previously described (Bhatt and Neckameyer, 2013) for 10 infected and 10 PBS treated larvae 24h post-treatment, over three replicates. The quantify of food in the guts of infected and challenged larvae was compared by feeding treated flies medium with 5% FD&C Blue #1 dye for 24hr. 10 guts were then dissected from each group, crushed with a piston pellet in 500μL of 1X PBS, and centrifuged before measuring the OD625 of the resulting samples. Five replicates were performed for both groups.

Immunohistochemistry and Fluorescence Imaging

Dissected *Drosophila* midguts were fixed in 4% paraformaldehyde in 1× PBS for 45 to 90 min and successively washed 3 times with 0.1% TritonX in PBS. Guts were then incubated for an hour in blocking solution (1% bovine serum albumin, 1% normal donkey serum, and 0.1% Triton X-100 in PBS). Overnight primary antibody staining was performed at room temperature (RT). Guts were washed 3 times with 0.1% TritonX in PBS and secondary antibody staining was performed for two or more hours in PBS. The exception to this procedure was staining against the Delta isotope, in which case an alternate blocking solution was used (3% bovine serum albumin and 0.1% Triton X-100 in PBS) for 3 h, and antibody staining was performed in 1% BSA and 0.1% Triton X-100 in PBS at 18°C. Primary antibodies used: rabbit anti-pH3 (1:000, Millipore Cat# 06-570, RRID:AB_310177), rabbit anti-β-Galactosidase (1:1000, MP Biomedicals Cat# 0855976, RRID:AB_2334934), goat anti-β-Galactosidase (1:1000, MP Biomedicals), mouse anti-Prospero (1:100, DSHB Cat# Prospero (MR1A), RRID:AB_528440), and mouse anti-Delta (1:100, DSHB Cat# c594.9b, RRID:AB_528194). Secondary antibodies used: donkey anti-rabbit-555 (1:2000, Thermo Fisher Scientific Cat# A-31572, RRID:AB_162543), donkey anti-goat-555 (1:2000, Thermo Fisher Scientific Cat# A-21432, RRID:AB_2535853), donkey anti-mouse-488 (1:2000, Thermo Fisher Scientific Cat# A-21202, RRID:AB_141607), and donkey anti-mouse-647 (1:1000, Thermo Fisher Scientific Cat# A-31571, RRID:AB_162542). DNA was stained in 1:50,000 DAPI (Sigma-Aldrich) in PBS for 30min, and samples received a final three washes in 1X PBS before mounting in antifade medium (Citifluor AF1). Imaging was performed on a Zeiss LSM 700 fluorescent-confocal inverted microscope.

Estimation of Total Midgut AMPs

AMP counting was performed on the guts of the larval progeny of esg^{TS} flies crossed to *Su(H)-lacZ* in order to visualize islet boundaries (by PCs) and individual AMPs. Total AMPs per gut (Figure 2G) were calculated by averaging the number of AMPs per islet in 105 islets from 8 UC guts and in 232 islets from 21 infected guts. The total number of islets present in each gut was also counted for all the guts of UC and *Ecc15* treated wL3 larvae.

Transcriptome Analysis

Oral infection of larvae was performed as previously described. 50 larval guts per condition were dissected 6h post-treatment and immediately transferred into Trizol (Life Technologies) kept on ice and subsequently homogenized, for a total of 3 replicates. Total RNA was isolated using a hybrid modified Trizol-Rneasy (Qiagen) extraction protocol. RNA underwent quantification and Quality check (QC) procedures via Fragment Analyzer (Advanced Analytical), before 3′ end RNA-seq libraries preparation. Following RNA extraction and QC, we utilized QuantSeq 3′ mRNA-Seq Library Prep Kit (Lexogen) to prepare 3′ end RNA-seq libraries. Libraries were again Qced with Fragment Analyzer before pooling and sequencing. Illumina NextSeq 500 platform using standard protocol for 75 bp single-end read sequencing at the Cornell Life Sciences Sequencing core facility was utilized to sequence libraries. 5 to 6 million reads were made per sample, which approximately equals a 20x coverage by conventional RNA-seq. Quality control of raw reads was performed with fastqc and reads were trimmed by trimmomatic and then mapped to the *Drosophila* transcriptome using STAR. Deseq2 was used for differential expression analysis and PCAs were performed using custom R scripts (available upon request). Gene Ontology was performed using the online tool Gorilla. Principal component analysis (PCA) showed that all three biological replicates clustered together, indicating good reproducibility of the response for each type of tissue sample, and demonstrated that, while the larval and adult midguts displayed differences in gene expression that accounts for most of the variance (separated by PC1, 82% of total variance), the remaining variance originated in a common response to infection (separated by PC2, 11% variance) (Figure 4A).

RT-qPCR

Total RNA was extracted from pools of ~20 dissected larval guts using a standard Trizol (Invitrogen) extraction. RNA samples were treated with PERFECTA DNase I (Quanta #95150-01K), and cDNA was generated using qScript cDNA Synthesis Kit (Quantabio # 95047-100). qPCR was performed using PerfeCTa® SYBR® Green FastMix® (Quanta Biosciences # 95072-012) in a Bio-Rad CFX-Connect instrument. Data represent the ratio between the Ct value of the target gene and that of the reference gene, RpL32 (also known as Rp49).

MARCM Clones

MARCM flies (Lee and Luo, 2001) were crossed to either *tkv*^{4} *FRT 40A* or *FRT 40A* control. We balanced the Bloomington stock *tkv*^{4} *FRT40A* over a *Cyo,GFP* balancer to select larvae containing the construct. Larvae were reared as described above. L1 larvae were heat shocked in a water bath at 37 °C for 1 h. Larvae were infected as described above and dissected at 24hrs post-infection.

QUANTIFICATION AND STATISTICAL ANALYSIS

All analyses were performed in Prism (GraphPad Prism V7.0a, GraphPad Software). For survival assays, the curves represent the average percent survival ±SE of three or more biological replicates (n = 20 flies for each biological replicate). A Log-rank test was used to determine significance (*$p < 0.05$ **$p < 0.01$ ***$p < 0.001$ ****$p < 0.0001$). In bacterial load quantification assays, the horizontal lines represent median values for each time point. Three biological replicates were included. Following normalization, results were analyzed using a two-way ANOVA followed with Sidak's post-tests for specific comparisons (*$p < 0.05$ **$p < 0.01$ ***$p < 0.001$ ****$p < 0.0001$). For all other experiments, mean values of three or more biological repeats are presented ±SE. Significance was calculated by a Student's t test following normalization (*$p < 0.05$ **$p < 0.01$ ***$p < 0.001$ ****$p < 0.0001$).

DATA AND CODE AVAILABILITY

The accession number for the raw RNA-seq data reported in the paper is NCBI BioProject: PRJNA553080.